CHEMISTRY
A EUROPEAN JOURNAL

FULL PAPER

DOI: 10.1002/chem.201300496

Chemisorption of Exchange-Coupled $[Ni_2L(dppba)]^+$ Complexes on Gold by Using Ambidentate 4-(Diphenylphosphino)benzoate Co-Ligands**

Matthias Golecki,[a] Jochen Lach,[a] Alexander Jeremies,[a] Frank Lungwitz,[b] Michael Fronk,[b] Georgeta Salvan,[b] Dietrich R. T. Zahn,[b] Jaena Park,[c, d] Yulia Krupskaya,[d] Vladislav Kataev,[d] Rüdiger Klingeler,[c] Bernd Büchner,[d] Benjamin Mahns,[d] Martin Knupfer,[d] Pablo F. Siles,[d, g] Daniel Grimm,[d, g] Oliver G. Schmidt,[d, g] Andreas Reis,[e] Werner R. Thiel,[e] Daniel Breite,[f] Bernd Abel,[f] and Berthold Kersting*[a]

Abstract: A new strategy for the fixation of redox-active dinickel(II) complexes with high-spin ground states to gold surfaces was developed. The dinickel(II) complex $[Ni_2L(Cl)]ClO_4$ (**1**ClO_4), in which L^{2-} represents a 24-membered macrocyclic hexaaza-dithiophenolate ligand, reacts with ambidentate 4-(diphenylphosphino)benzoate (dppba) to form the carboxylato-bridged complex $[Ni_2L(dppba)]^+$, which can be isolated as an air-stable perchlorate $[Ni_2L(dppba)]ClO_4$ (**2**ClO_4) or tetraphenylborate $[Ni_2L(dppba)]BPh_4$ (**2**BPh_4) salt. The auration of **2**ClO_4 was probed on a molecular level, by reaction with AuCl, which leads to the monoaurated $Ni^{II}{}_2Au^I$ complex $[Ni^{II}{}_2L(dppba)Au^ICl]ClO_4$ (**3**ClO_4). Metathesis of **3**ClO_4 with $NaBPh_4$ produces $[Ni^{II}{}_2L(dppba)Au^IPh]BPh_4$ (**4**BPh_4), in which the Cl^- is replaced by a Ph^- group. The complexes were fully characterized by ESI mass spectrometry, IR and UV/Vis spectroscopy, X-ray crystallography (**2**BPh_4 and **4**BPh_4), cyclic voltammetry, SQUID magnetometry and HF-ESR spectroscopy. Temperature-dependent magnetic susceptibility measurements reveal a ferromagnetic coupling $J = +15.9$ and $+17.9\ cm^{-1}$ between the two Ni^{II} ions in **2**ClO_4 and **4**BPh_4 ($H = -2JS_1S_2$). HF-ESR measurements yield a negative axial magnetic anisotropy ($D < 0$), which implies a bistable (easy axis) magnetic ground state. The binding of the $[Ni_2L(dppba)]ClO_4$ complex to gold was ascertained by four complementary surface analytical methods: contact angle measurements, atomic-force microscopy, X-ray photoelectron spectroscopy, and spectroscopic ellipsometry. The results indicate that the complexes are attached to the Au surface through coordinative Au–P bonds in a monolayer.

Keywords: chemisorption · gold · ligands · macrocyclic ligands · nickel · phosphorus heterocycles

[a] M. Golecki, J. Lach, A. Jeremies, Prof. Dr. B. Kersting
Institut für Anorganische Chemie
Universität Leipzig, 04103 Leipzig (Germany)
Fax: (+49) 341-973-6199
E-mail: b.kersting@uni-leipzig.de

[b] F. Lungwitz, Dr. M. Fronk, Prof. Dr. G. Salvan, Prof. Dr. D. R. T. Zahn
Semiconductor Physics Institute
Chemnitz University of Technology
09107 Chemnitz (Germany)

[c] J. Park, Prof. Dr. R. Klingeler
Kirchhoff Institute for Physics, University of Heidelberg
69120 Heidelberg (Germany)

[d] J. Park, Dr. Y. Krupskaya, Dr. V. Kataev, Prof. Dr. B. Büchner, B. Mahns, Prof. Dr. M. Knupfer, Dr. P. F. Siles, Dr. D. Grimm, Prof. Dr. O. G. Schmidt
Leibniz Institute for Solid State and Materials Research
IFW Dresden, 01171 Dresden (Germany)

[e] A. Reis, Prof. Dr. W. R. Thiel
Fachbereich Chemie, Technische Universität Kaiserslautern
Erwin Schrödinger Strasse 54, 67663 Kaiserslautern (Germany)

[f] D. Breite, Prof. Dr. B. Abel
Chemische Abteilung, Leibniz-Institut für Oberflächenmodifizierung e. V.
04318 Leipzig (Germany)

[g] Dr. P. F. Siles, Dr. D. Grimm, Prof. Dr. O. G. Schmidt
Material Systems for Nanoelectronics
Chemnitz University of Technology
Reichenhainerstrasse 70, 09107 Chemnitz (Germany)

[**] dppba = 4-(diphenylphosphino)benzoate.

Supporting information for this article (including X-ray crystallographic data of **2**ClO_4 and **4**BPh_4 in the CIF format and XPS spectra) is available on the WWW under http://dx.doi.org/10.1002/chem.201300496.

Introduction

The deposition of magnetically or electronically bistable transition-metal complexes on planar surfaces in which the spatially addressable functional units are assembled at the molecular level is an attractive research field,[1,2] and has perspectives for the storage of information at the molecular level[3,4] and in molecular electronics.[5–10] Most research to date has focused on the physisorption or chemisorption of phthalocyanines,[11] porphyrines,[12] spin-crossover compounds, and more recently also single molecule magnets,[13,23] and several strategies have been developed to obtain these materials as rows,[14] thin films,[15,16] or multilayers.[17] The thermal evaporation of polynuclear transition-metal complexes, however, has found limited applicability in surface deposition due to their limited thermal and kinetic stability,[18] and so new solution-based methods for surface functionalization had to be devised. Due to the high affinity of thiolates for gold,[19,20] the ease of Au–S bond formation (i.e., deposition of thiols from solution) and the possibility of surface patterning by soft-lithography,[21] the surface fixation of open-shell transition-metal complexes bearing thiol functions have therefore become the focus of intense investigations.

Two major strategies have evolved in the field of molecular magnetism that allow the deposition of polynuclear transition-metal carboxylato complexes with single molecule magnetism (SMM) behavior on gold. In the first approach, a self-assembled monolayer of a bifunctional thiol HS–X–L is prepared (L is usually a carboxylate function, whereas X is a spacer), which is then reacted with the carboxylato cluster by using a ligand exchange reaction.[22] In the second approach, a SMM molecule with a properly functionalized ligand shell is directly deposited.[23,24] Both strategies have their advantages and disadvantages. In the latter method, for example, the thiol has to be protected as it reacts with the cluster core. The solution methods have the advantage that they can be applied to more relevant substrates, like silicon, silicon oxides, or ferromagnetic metal oxides (such as $La_{0.7}Sr_{0.3}MnO_3$).

Our team is interested in the synthesis and characterization of exchange-coupled transition-metal complexes stabilized by macrocyclic polyaza-polythiophenolate ligands. Particularly well-investigated are dinuclear complexes of the N_6S_2 macrocycle H_2L (Figure 1).[25,26] The N_6S_2 macrocycle supports mixed-ligand complexes of the type $[M_2L(L')]^{n+}$ with a doubly thiolato-bridged $N_3M(\mu\text{-}SR)_2(\mu\text{-}L')MN_3$ core structure. The complexes are distinguished by the fact that the co-ligand L′ is readily exchanged. Thus, a large number of closely related $[Ni^{II}_2L(\mu\text{-}L')]^+$ complexes (e.g., $L' = Cl^-$, OH^-, SH^-, NO_2^-, NO_3^-, N_3^-, N_2H_4, $CH_3CO_2^-$, HCO_3^-, $H_2PO_4^-$, ClO_4^-, ReO_4^-, CrO_4^{2-}, MoO_4^{2-}, WO_4^{2-}, alkyl carbonates ($ROCO_2^-$), alkyl carbamates ($RNCO_2^-$), pyrazolate, tetrazolate, and tetrahydridoborate (BH_4^-)) were prepared and their stability,[27,28] reactivity,[29,30] and electronic structures[31,32] were studied as a function of the type of co-ligand and oxidation state.

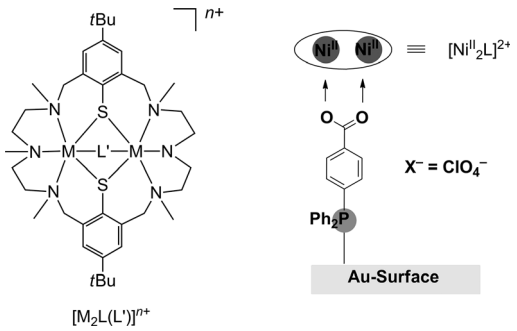

Figure 1. Left: Structure of dinuclear complexes $[M_2L(L')]^+$ of the macrocyclic ligand H_2L. Right: Sketch of a chemisorbed $[Ni_2L(O_2CC_6H_4PPh_2)]ClO_4$ complex on a gold surface.

Since the magnetic properties of the $[Ni_2L(L')]^+$ complexes can be switched by using chemical[33,34] or electrochemical methods,[35] we became interested in the immobilization of such complexes on surfaces. We designed a strategy that is based on the direct deposition of SMMs on surfaces. We anticipated that the $[LNi_2]^{2+}$ fragment would react with the hard donor function (H) of an ambidentate coligand H–Y–S to form a well-defined and isolable $[LNi_2(H–Y–S)]^+$ complex as shown in Figure 1. The macrocyclic supporting ligand L was expected to impose thermodynamic and kinetic stability on the complex, thus preventing a backbiting of the soft donor function (S) with the cluster core. The soft phosphine donor in the precursor $[LNi_2(H–Y–S)]^+$ would then bind to the gold surface.[36,37] Notice the salt-like composition of the adsorbate, containing monocations and anions. Thus, the anion is deposited along with the cation, but is only physisorbed.

The present study focuses on the ambidentate 4-(diphenylphosphino)benzoate ligand (Hdppba)[38] with a soft diphenylphosphine and a hard carboxylate function. We report the preparation and isolation of the complex salts $[Ni_2L(dppba)]ClO_4$ and $[Ni_2L(dppba)]BPh_4$, their successful auration with AuCl, and their chemisorption on gold. The crystal structures, electrochemistry, reactivity features, magnetic and electrochemical properties of the complexes are described, as are the results of four complementary surface analytical methods: contact angle measurements, atomic-force microscopy, X-ray photoelectron spectroscopy, and ellipsometry. The coordination chemistry of transition-metal complexes with phosphine complexes is well-established. Phosphine-protected gold nanoparticles were reported.[39–44] Little work has been performed in the field of phosphines adsorbed on gold surfaces;[36,37,45] to the best of our knowledge, this is the first approach for the chemisorption of exchange coupled metal clusters through ambidentate phosphine-carboxylate ligands.

Results and Discussion

Synthesis and characterization of metal complexes: The synthetic procedures are summarized in Scheme 1. Treatment

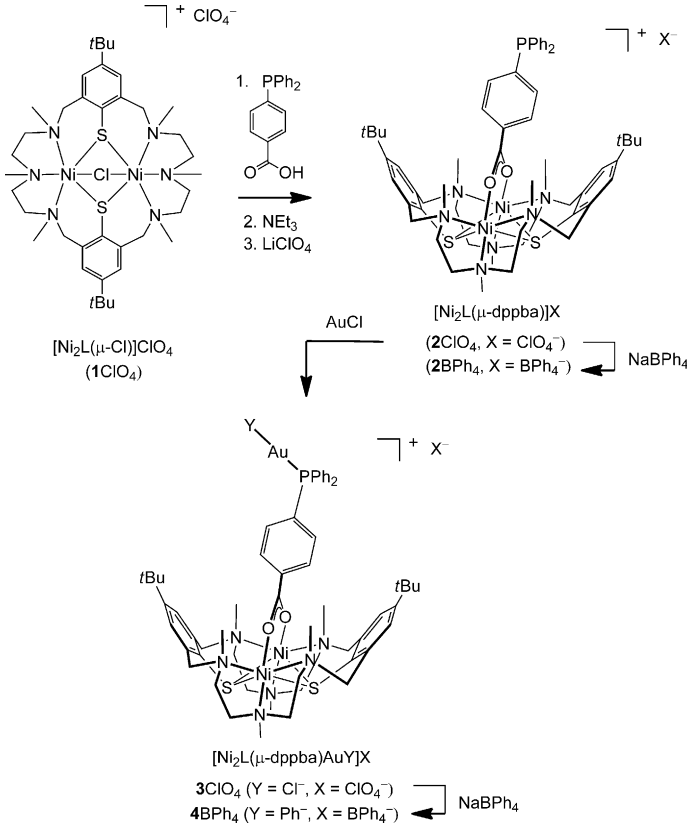

Scheme 1. Preparation of complexes **2**–**4**.

of $[Ni_2L(\mu\text{-Cl})]ClO_4$ (**1**ClO_4)[46] with 4-(diphenylphosphino)-benzoic acid in MeOH in the presence of NEt_3 under Ar provides a green solution from which upon addition of $LiClO_4$ the green, air-sensitive target compound, $[Ni_2L(\mu\text{-dppba})]ClO_4$ (**2**ClO_4) precipitates in 86% yield. The electrospray ionization mass spectrum (ESI-MS) of a dilute methanol solution of **2**ClO_4 exhibited a molecular ion peak for $[Ni_2L(\mu\text{-dppba})]^+$ ($m/z = 1089.4$), and the combustion analysis agreed well with the formula **2**ClO_4. The presence of two IR absorption bands at 1550 cm^{-1} ($\nu_{as}(RCO_2^-)$) and 1408 cm^{-1} ($\nu_s(RCO_2^-)$) are indicative of a bridging carboxylate function as anticipated. Electronic absorption bands at 650 and 1122 nm attributable to spin-allowed ν_2 and ν_1 transitions of a six-coordinated $NiN_3S_2O^{carboxylate}$ chromophore suggest that this structure is maintained in the solution state as well.[28]

Efforts to obtain single crystals of **2**ClO_4 suitable for X-ray diffraction analysis were unsuccessful.[47] However, such crystals could be obtained in the case of the tetraphenylborate salt **2**BPh_4 which was synthesized by metathesis of **2**ClO_4 with $NaBPh_4$. Figure 2 shows that the dppba ligand bridges the two Ni^{II} ions through its carboxylate function, in a symmetrical fashion leading to a Ni···Ni distance of 3.481(2) Å. The benzoate group of the dppba ligand is long enough so that the P atom is exposed out of the binding pocket of the $[Ni_2L]^{2+}$ fragment. In addition, the C-P-C angles in **2**ClO_4 (101.1, 101.7, and 106.5°) are very similar to

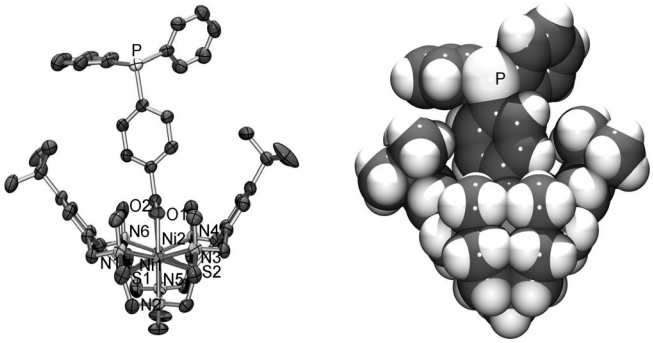

Figure 2. ORTEP (left) and van der Waals plot (right) of the molecular structure of the $[Ni_2L(O_2CC_6H_4PPh_2)]^+$ cation in crystals of **2**BPh_4. Thermal ellipsoids are at 50% probability. Selected bond lengths [Å] and angles [°]: Ni1-O1 1.984(3), Ni1-N1 2.265(4), Ni1-N2 2.138(4), Ni1-N3 2.301(4), Ni1-S1 2.4742(13), Ni1-S2 2.4434(14), Ni2-O2 2.039(3), Ni2-N4 2.266(4), Ni2-N5 2.135(3), Ni2-N6 2.273(4), Ni2-S1 2.4713(16), Ni2-S2 2.4757(14); Ni2-S1-Ni1 89.47(5), Ni1-S2-Ni2 90.08(5).

those in PPh_3 (103.3, 103.3, and 101.7°)[48] indicating that the structure of the dppba ligand is not markedly perturbed by the $[Ni_2L]^{2+}$ fragment. To our knowledge, there are not many paramagnetic 3d metal complexes of the dppba ligand. However, the Walton group reported a number of multiply bonded dimolybdenum and dirhenium complexes with this ligand.[49] Overall, the $[Ni_2L]^{2+}$ complex binds the dppba selectively through the carboxylate function in a chelating manner leaving an uncoordinated P atom for anchoring to metal surfaces.

We decided to examine the aurophilicity[50] of the $[Ni_2L(dppba)]ClO_4$ salt prior to surface deposition studies, by treating it with suitable gold(I) compounds. An aurated species was also sought for as a reference compound in the XPS studies. $[Ni_2L(dppba)]^+$ has three potential gold binding sites, the two thiolate sulfur atoms from the macrocycle L^{2-} and the exposed P atom from the dppba ligand. No apparent color changes took place when **2**ClO_4 was allowed to react with AuCl in a 1:1 ratio in CH_2Cl_2 for 24 h (Scheme 1), however, an ESI-MS spectrum of the green reaction mixture showed the presence of a new species, formulated as the monogold(I) adduct $[Ni_2L(dppba)AuCl]^+$ (**3**, $m/z = 1321.4$), which can be isolated as a perchlorate salt **3**ClO_4 in 91% yield. The addition of further equivalents of AuCl to **2**ClO_4 or **3**ClO_4 did not result in a polyaurated species,[51] which shows that there is indeed only one gold binding site in **2**.

Unfortunately, we were not successful in growing single crystals of **3**ClO_4. However, crystals of the tetraphenylborate salt of the related complex $[Ni_2L(dppba)AuPh]BPh_4$ (**4**BPh_4), which is accessible by metathesis of **3**ClO_4 with $NaBPh_4$ (Scheme 1), can be obtained by recrystallization from a mixed $CHCl_3/CH_2Cl_2$/hexanes solution. Notice that the gold-bound chlorido ligand is replaced by a phenyl group in this reaction. The ability of the $[BPh_4]^-$ ion to transfer a phenyl group is not unusual[52,53] and some of these reactions occur even in aqueous solution.[54] The phenyl compound is formed in high yield and is air stable.

The crystal structure determination of $4BPh_4{\cdot}3CH_2Cl_2{\cdot}CHCl_3{\cdot}H_2O$ revealed the presence of two crystallographically independent but chemically identical molecules A and B of the trinuclear $[Ni_2L(dppba)AuPh]^+$ complex **4**. A perspective drawing of one of them is shown in Figure 3, whereas selected bond lengths and angles are

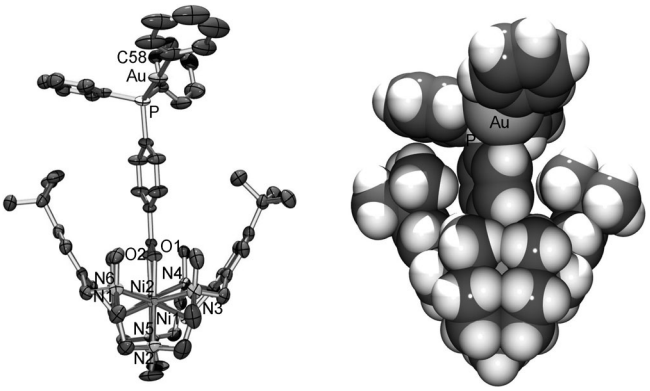

Figure 3. ORTEP (left) and van der Waals plot (right) of the molecular structure of the $[Ni_2L(dppba)AuPh)]^+$ cation (molecule A) in crystals of $4BPh_4{\cdot}3CH_2Cl_2{\cdot}CHCl_3{\cdot}H_2O$. Thermal ellipsoids are at 50% probability. Selected bond lengths [Å] and angles [°] for molecule a [molecule b]: Au-C58 2.048(7) [2.041(5)], Au-P 2.3013(13) [2.294(1)], Ni1-O1 2.004(3) [2.002(3)], Ni1-N1 2.259(4) [2.215(4)], Ni1-N2 2.144(4) [2.127(4)], Ni1-N3 2.276(5) [2.335(4)], Ni1-S1 2.482(2) [2.465(1)], Ni1-S2 2.469(1) [2.474(2)], Ni2-O2 2.019(3) [2.031(3)], Ni2-N4 2.232(4) [2.223(4)], Ni2-N5 2.138(4) [2.165(4)], Ni2-N6 2.329(4) [2.298(4)], Ni2-S1 2.459(1) [2.444(2)], Ni2-S2 2.478(2) [2.496(1)]; C58-Au-P 177.82(18) [175.73(14)], Ni2-S1-Ni1 89.16(4) [89.54(5)], Ni1-S2-Ni2 88.99(5) [88.16(4)].

given in the Figure caption. The complexes are well separated from each other. The Au^I–Ph fragment is attached to the terminal phosphorus atom of the dppba co-ligand.[55] The coordination geometry of the gold atom is almost perfectly linear, with the C-Au-P angle being 177.8(2)°. The Au–C and Au–P bond lengths are 2.048(7) and 2.3013(12) Å, respectively. The bond lengths and angles in **4** are very similar to those in $[Au(Ph)(PPh_3)]$ (Au–C 2.045(6), Au–P 2.296(2) Å, P-Au-C 175.5(2)°).[56] Notice that the binding of the $[AuPh]^+$ fragment does not significantly alter the structure of the $[Ni_2L(dppba)]^+$ complex. The main difference is the smaller twist angle (14°) between the planes through the aromatic ring of the benzoate moiety and the carboxylato group. The orientation of the PPh_2 group with respect to the *tert*-butyl substituents is also different in **4**, indicating that the Ph_2P group can freely rotate around the $Ph_2P–C_6H_4CO_2$ bond. The cleft-like structure of the complex cations appears to be of importance in the binding to the gold surface. In fact, the cleft, which holds the ambidentate co-ligand, directs the complexes to bind to the surface in an "upside-down" fashion. In summary, the diphenylphosphino group in $\mathbf{2}ClO_4$ is the only potential binding site for gold atoms, and the binding does not alter the overall structure of the $[Ni_2L]^{2+}$ fragment.

Cyclic voltammetry: Cyclic voltammetry (CV) experiments were carried out to investigate the redox behavior of $[Ni_2L(dppba)]ClO_4$ ($\mathbf{2}ClO_4$), $[Ni_2L(pdbba)AuCl]ClO_4$ ($\mathbf{3}ClO_4$), and $[Ni_2L(pdbba)AuPh]BPh_4$ ($\mathbf{4}BPh_4$). Figure 4 shows the cyclic voltammograms of solutions of these compounds in CH_2Cl_2. The CV of the acetato-bridged complex $[Ni_2L(OAc)]ClO_4$ was reported previously,[57] and is included for comparison.

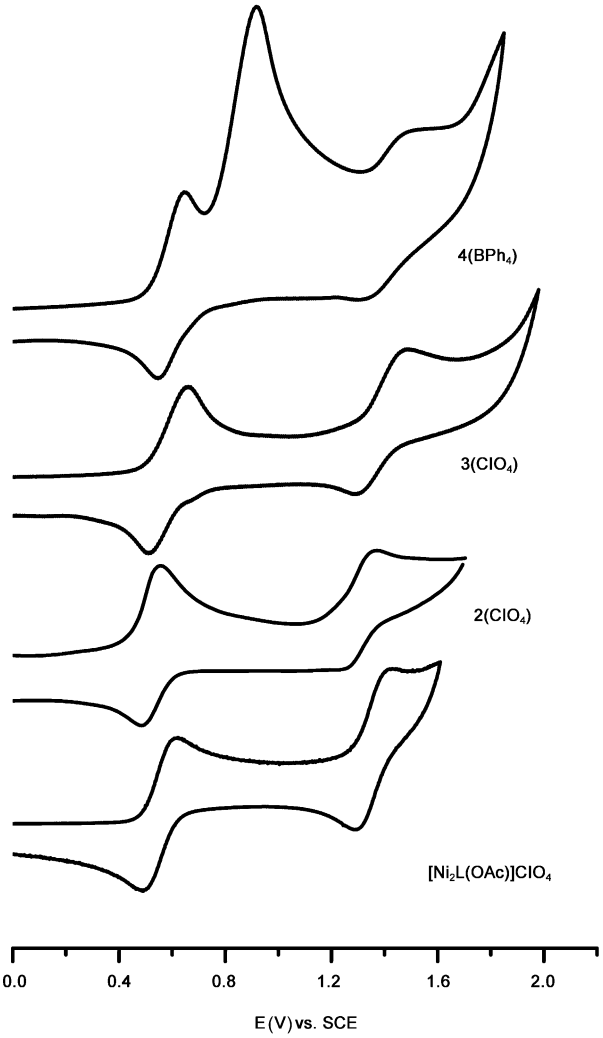

Figure 4. Cyclic voltammogram of $\mathbf{2}ClO_4$–$\mathbf{4}ClO_4$ (in CH_2Cl_2) and $[Ni_2L(OAc)]ClO_4$ (in CH_3CN) at 298 K. Experimental conditions: 0.1 M [n-$Bu_4N]PF_6$, sample concentration of approximately 1×10^{-3} M, Pt disk working electrode, Ag wire reference electrode, scan rate = 100 mV s^{-1}, $[Co(Cp_2)]PF_6$ internal reference.

The CV of $\mathbf{2}ClO_4$ shows two redox waves, one at $E^1_{1/2} = +0.52$ V (vs. a saturated calomel electrode (SCE)) with a peak-to-peak separation ΔE_p of 0.07 V and one at $E^2_{1/2} = +1.31$ V with $\Delta E_p = 0.10$ V. The first oxidation is a one-electron process as confirmed by controlled potential coulometry at 273 K. Thus, the oxidation of $[Ni_2L(dppba)]ClO_4$ at an applied potential of +1.0 V versus SCE in CH_3CN solution consumed $n = 0.95$ e$^-$ per complex, whereas re-reduction at 0.0 V versus SCE caused transfer of 96% of the charge

passed in oxidation. In addition, the CV of the electrogenerated $[Ni_2L(dppba)]^{2+}$ dication is identical to that of the parent $[Ni_2L(dppba)]^+$ monocation.

The electrochemical behavior of $[Ni_2L(dppba)]^+$ is similar to that of the acetato-bridged complex $[Ni_2L(OAc)]ClO_4$, which shows two redox waves at $E^1_{1/2}=0.56$ V and $E^2_{1/2}=1.36$ V.[56] The redox waves can be assigned to metal-centered ($Ni^{II}Ni^{II}\rightarrow Ni^{II}Ni^{III}$) and ligand-based oxidations (RS^-(thiolate)$\rightarrow RS^\bullet$ (thiyl radical)) within the $[Ni_2L]^{2+}$ unit as represented in Equations (1) and (2).[58]

Similarly, for $\mathbf{3}ClO_4$ two redox waves are observed at $E^1_{1/2}=0.59$ V ($\Delta E_p=0.14$ V) and $E^2_{1/2}=1.38$ V ($\Delta E_p=0.13$ V) indicative of the same redox behavior. The first oxidation yields a mixed-valent $Ni^{II}Ni^{III}Au^I$ complex $\mathbf{3}^{2+}$ as indicated in Equation (3)[59] and the second oxidation is ligand centered. The small shift to more anodic potentials is presumably a consequence of an electron-withdrawing effect of the AuCl unit. This decreases the electron density of the carboxylate function, which increases the stability of the $Ni^{II}Ni^{II}$ form to some extent. For $\mathbf{4}BPh_4$, the same is evident, with the $E^1_{1/2}$ and $E^2_{1/2}$ values of 0.59 V ($\Delta E_p=0.10$ V) and 1.4 V ($\Delta E_p=0.16$ V). The irreversible redox wave at 0.91 V is attributed to an oxidation of the tetraphenylborate anion.

The dication $\mathbf{3}^{2+}$ can also be prepared by chemical oxidation. Green solutions of $\mathbf{3}ClO_4$ turn dark red upon addition of one equivalent of $Cu(ClO_4)_2$. The UV/Vis spectra of such solutions reveal several strong absorption bands ($\lambda_{max}=782$ (4945), 517 (2735), 397 (2998), 330 (9864), and 304 nm ($13560\,M^{-1}cm^{-1}$) attributable to ligand-to-metal ($RS^-\rightarrow Ni^{III}$) charge-transfer transitions. The same absorption features are observed for electrochemically generated solutions of $\mathbf{3}^{2+}$, showing that both processes produce the same species. Interestingly, there is also a feature at 1590 nm ($2538\,M^{-1}cm^{-1}$) attributable to an intervalence transition. Electrospray ionization mass spectrometry provided final conformation for the identity of the dication $\mathbf{3}^{2+}$, with a peak at $m/z=1420.29$ for a mixed-valent $[Ni^{II}Ni^{III}L(dppba)AuCl](ClO_4)^+$ monocation and a peak at $m/z=661.61$ for the mixed-valent $[Ni^{II}Ni^{III}L(dppba)AuCl]^{2+}$ dication.

$$[Ni^{II}Ni^{II}L(dppba)]^+ \underset{+e^-}{\overset{-e^-}{\rightleftharpoons}} [Ni^{II}Ni^{III}L(dppba)]^{2+} \quad (1)$$
$$\mathbf{2}^+ \qquad\qquad \mathbf{2}^{2+}$$

$$[Ni^{II}Ni^{III}L(dppba)]^{2+} \underset{+e^-}{\overset{-e^-}{\rightleftharpoons}} [Ni^{II}Ni^{III}L^\bullet(dppba)]^{3+} \quad (2)$$
$$\mathbf{2}^{2+} \qquad\qquad \mathbf{2}^{3+}$$

$$[Ni^{II}Ni^{II}L(dppba)AuX]^+ \underset{+e^-}{\overset{-e^-}{\rightleftharpoons}} [Ni^{II}Ni^{III}L(dppba)AuX]^{2+} \quad (3)$$
$$\mathbf{3}^+ \qquad\qquad \mathbf{3}^{2+}\ (3a,\ X = Cl)$$
$$\mathbf{4}^+ \qquad\qquad \mathbf{4}^{2+}\ (3b,\ X = Ph)$$

$$[Ni^{II}Ni^{III}L(dppba)AuX]^{2+} \underset{+e^-}{\overset{-e^-}{\rightleftharpoons}} [Ni^{II}Ni^{III}L^\bullet(dppba)AuX]^{3+} \quad (4)$$
$$\mathbf{3}^+ \qquad\qquad \mathbf{3}^{3+}\ (4a,\ X = Cl)$$
$$\mathbf{4}^+ \qquad\qquad \mathbf{4}^{2+}\ (4b,\ X = Ph)$$

The redox chemistry of the two-coordinate Au^I complexes was investigated by other research groups. Au^I complexes with mixed Cl^- and PPh_3 donor ligands generally undergo an irreversible reduction to Au^0 at cathodic potentials of less than -2 V.[60,61] The form and position of the reduction peaks also depend on the Au coverage of the electrode. For the present Ni_2Au complexes there are no redox waves in a potential window ranging from -2 to $+2.5$ V versus SCE that can be attributed to reduction of the dppba-Au^IPh group, which is in good agreement with the reported trend.[60] It can be concluded that this unit is redox inactive in this potential range. The +III oxidation level is common in nickel thiolate chemistry, and several other mixed-valent nickel thiolate complexes have been reported in the past two decades.[62–66] However, to our knowledge, trinuclear $Ni^{II}Ni^{III}Au^I$ species are not described nor reported in the literature yet.

Magnetic properties of $\mathbf{2}ClO_4$ and $\mathbf{4}BPh_4$: *Static magnetization measurements*: Static magnetization measurements for the paramagnetic $Ni^{II}{}_2$ and $Ni^{II}{}_2Au^I$ complexes $\mathbf{2}ClO_4$ and $\mathbf{4}BPh_4$ were performed with a commercial SQUID (superconducting quantum interference device) magnetometer from Quantum Design in the temperature range from 2 to 300 K in magnetic fields from 0 to 5 T. Figure 5 shows the

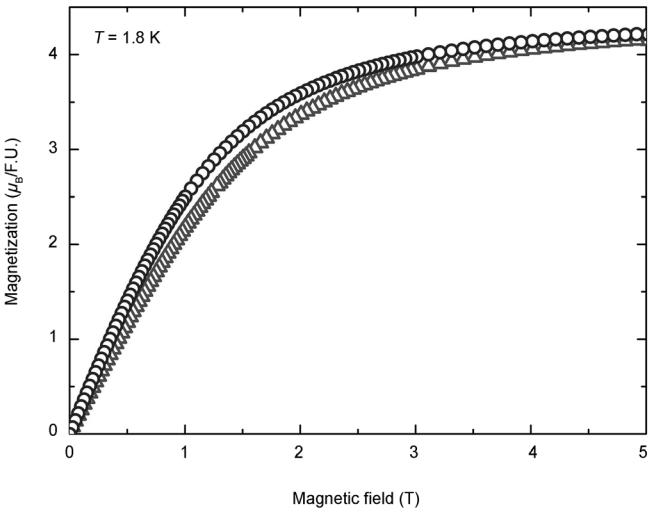

Figure 5. Magnetic field dependence of the static magnetization of $\mathbf{2}ClO_4$ (△) and $\mathbf{4}BPh_4$ (○) measured at $T=1.8$ K.

field dependence of the magnetization of $\mathbf{2}ClO_4$ and $\mathbf{4}BPh_4$ measured at $T=1.8$ K. The saturation magnetization is similar for the two complexes and is around 4.2 μ_B. This value corresponds to a total spin $S_{tot}=2$ in the ground state and indicates a ferromagnetic coupling between Ni^{2+} ions ($3d^8$, $S_{Ni}=1$) in both complexes.

Figure 6 shows the temperature dependence of the magnetic susceptibility $\chi(T)=M(T)/B$ and the inverse susceptibility $\chi^{-1}(T)$ of both complexes in an applied magnetic field

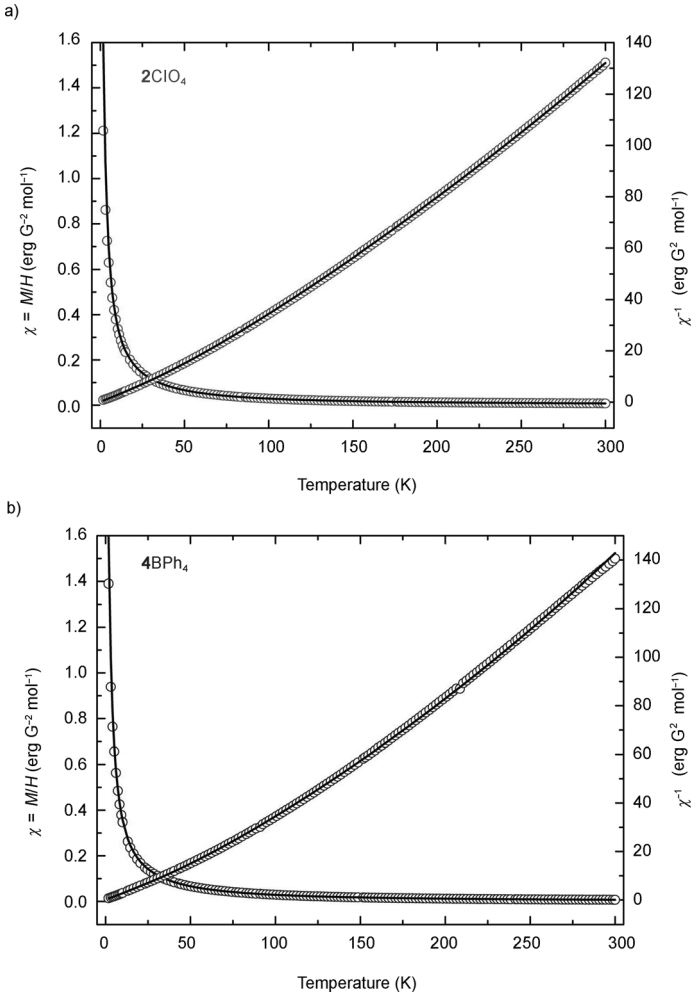

Figure 6. Temperature dependence of the static magnetic susceptibility, $\chi = M/B$ and the inverse susceptibility χ^{-1} of a) $\mathbf{2}ClO_4$ and b) $\mathbf{4}BPh_4$ measured at $B = 1$ T. Black lines correspond to the result of the fitting using the Hamiltonian [Eq. (5)] and ○ = data.

of 1 T. The data were analyzed using the Hamiltonian in Equation (5):

$$H = -2J\vec{S}_1 \bullet \vec{S}_2 + \mu_B \sum_{i=1}^{2} g\vec{S}_i \bullet \vec{B} + \sum_{i=1}^{2} D_i \left[S_{z,i}^2 - \frac{1}{3} S_i(S_i+1) \right] \quad (5)$$

in which the first term describes the isotropic magnetic coupling between the two Ni ions. Here, J is the Heisenberg exchange constant and S_1 and S_2 are the spin operators. The second term describes the Zeeman interaction with the magnetic field B and the last term describes the single ion anisotropy of the Ni ions. Here, g denotes the isotropic g-factor of the ion, μ_B is the Bohr magneton, B is the external magnetic field and D_i is the axial single-ion anisotropy constant. Based on those parameters, the susceptibility $\chi(T)$ and the inverse susceptibility $\chi^{-1}(T)$ were simulated by using the julX simulation program.[67] The values of the g-factor and of the magnetic anisotropy parameter D were taken from the ESR measurements (see below). We have found, however, that taking into account the D parameter does not change the result of the fit of the susceptibility data, which is most likely related to the smallness of the D value.[68] The modeling reveals a ferromagnetic coupling of 23 (16 cm^{-1}) and 26 K (18 cm^{-1}) between the two Ni ions for $\mathbf{2}ClO_4$ and for $\mathbf{4}BPh_4$, respectively. These values agree well with those of other carboxylato-bridged Ni^{II}_2 complexes bridged by the hexaaza-dithiophenolate macrocycle.[33]

High-field electron spin resonance (HF-ESR) measurements: High-field ESR (HF-ESR) measurements were performed on $\mathbf{2}ClO_4$ and $\mathbf{4}BPh_4$ with a homemade spectrometer on the basis of a Millimeterwave Vector Network Analyzer from AB Milimetre.[69] The samples were measured as oriented powders in magnetic fields up to 15 T for excitation frequencies $\nu = 80$–350 GHz. The typical ESR spectra of $\mathbf{2}ClO_4$ and $\mathbf{4}BPh_4$ at different temperatures and a frequency of 332 GHz are plotted in Figure 7. The spectra of both compounds look very similar. At $T = 4$ K we observe a single resonance line in the ESR spectrum, however, at higher T the number of lines increases. Above $T = 20$ K we observe four resonance lines corresponding to the transitions within the ground state multiplet $S = 2$. Such a transfer of the spectral weight to lower magnetic field with decreasing the temperature is the first indication for an axial magnetic anisotropy of the molecules ($D < 0$).

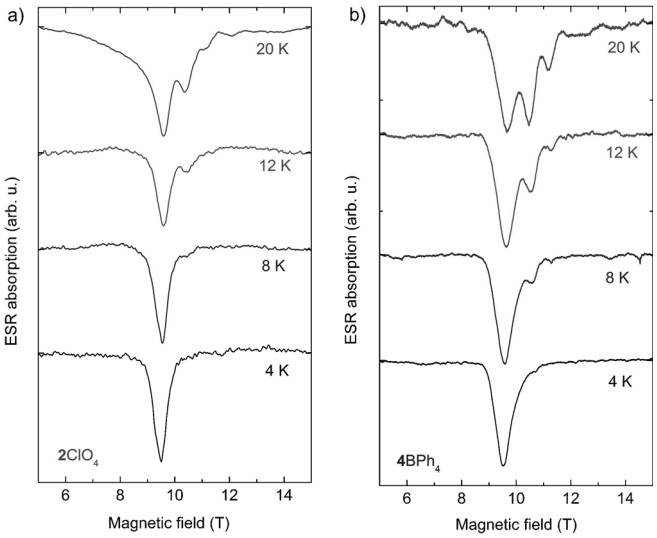

Figure 7. The temperature dependence of the ESR spectra of a) $\mathbf{2}ClO_4$ and b) $\mathbf{4}BPh_4$ at $\nu = 332$ GHz.

Figure 8 shows the frequency versus resonance field dependencies for $\mathbf{2}ClO_4$ and $\mathbf{4}BPh_4$ together with representative ESR spectra. The slopes of the four resonance branches in both cases reveal a g-factor of 2.17. By the extrapolation of the first resonance branch (line 1) to the zero field, the magnetic anisotropy of both compounds was estimated. We

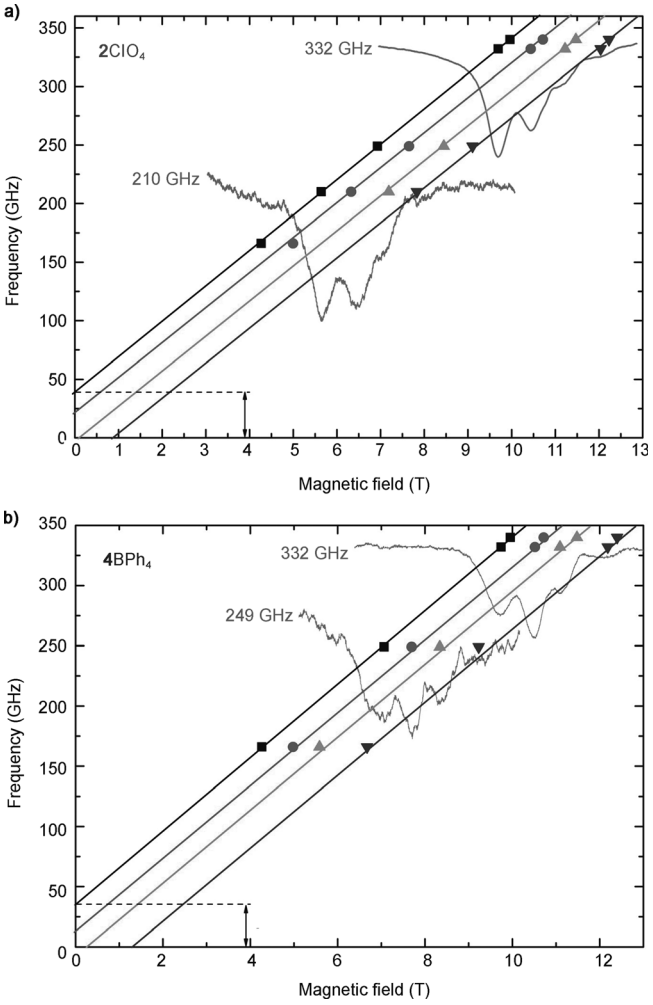

Figure 8. The frequency dependence of the ESR spectrum of a) $\mathbf{2}ClO_4$ at $T=20$ K ($\Delta=40$ GHz) and b) $\mathbf{4}BPh_4$ at $T=25$ K ($\Delta=35$ GHz; $g=2.17$ for both). ■ = Line 1; ● = line 2; ▲ = line 3; and ▼ = line 4.

find anisotropy gaps of 40 and 35 GHz for $\mathbf{2}ClO_4$ and $\mathbf{4}BPh_4$, respectively.

For the analysis of the ESR spectra we introduced a model that describes only the ground state of the molecule. The effective spin Hamiltonian in this case can be written as Equation (6):

$$H = g\mu_B \vec{S} \bullet \vec{B} + D\left[S_z^2 - \frac{1}{3}S(S+1)\right] \qquad (6)$$

in which the first term describes the Zeeman interaction of the total spin of the molecule with the magnetic field B and the second term describes the magnetic anisotropy of the molecule. We assume that each molecule has a single total spin $S=2$, a g-factor of 2.17, and a magnetic anisotropy parameter $D=\Delta/(S^2-(S-1)^2)$, which amounts to -13.3 GHz (-0.063 K) for $\mathbf{2}ClO_4$ and -11.6 GHz (-0.056 K) for $\mathbf{4}BPh_4$.

The simulation of the ESR spectra was performed for $\nu=$ 332 GHz, $T=20$ K and parallel orientation of the magnetic anisotropy axis to the applied magnetic field. The experimental and modeled ESR spectra are plotted in Figure 9 with the calculated energy-level diagram. As can be seen,

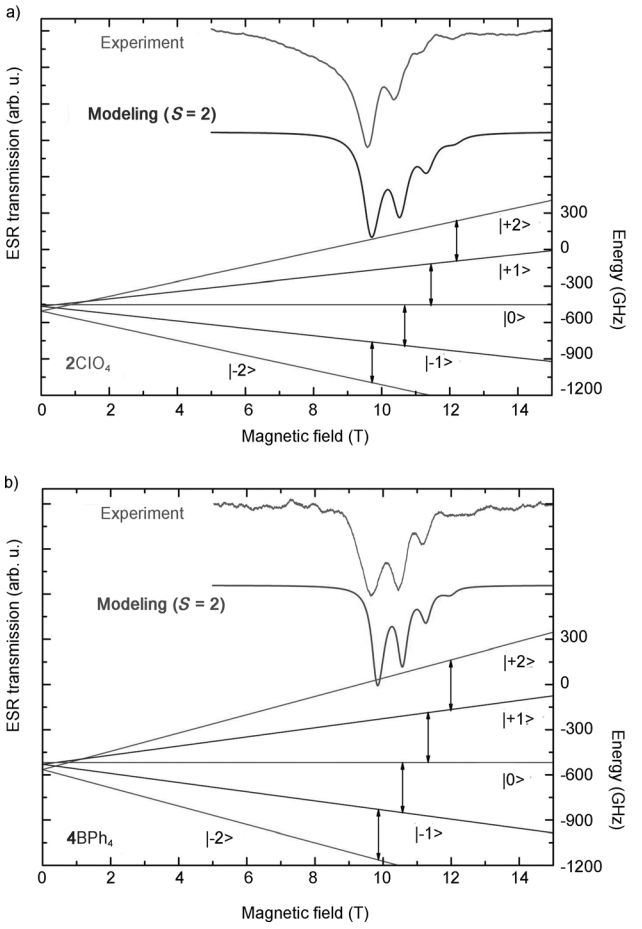

Figure 9. Experimental and modeled ESR spectra at $\nu=332$ GHz, $T=$ 20 K and corresponding energy-level diagrams for a) $\mathbf{2}ClO_4$ and b) $\mathbf{4}BPh_4$.

the simulation reproduces the experimental ESR spectra very well. The modeling confirms the negative sign of the axial magnetic anisotropy parameter ($D<0$) and the D values of -13.3 GHz (-0.063 K) and -11.6 GHz (-0.056 K) for $\mathbf{2}ClO_4$ and $\mathbf{4}BPh_4$, respectively. Overall, the magnetization and ESR measurements show no significant difference between compounds $\mathbf{2}ClO_4$ and $\mathbf{4}BPh_4$. The magnetic properties of **2** are not significantly changed upon attachment of the Au to the phosphorus atom. On the other hand, it is also clear that the magnetic anisotropy barrier is too small for getting sufficient retention of magnetization at finite temperature.

Chemisorption of $\mathbf{2}ClO_4$ on gold: To test whether $\mathbf{2}ClO_4$ can be immobilized on surfaces, it was brought in contact with a planar gold substrate. The deposition of the $[Ni_2L(dppba)]ClO_4$ complex salt with its pendant PPh_2 group was performed in analogy to the preparation of self-assembled

thiol monolayers on gold as described in the literature.[70] A clean gold-coated Si wafer was immersed in a 1×10^{-3} M solution of **2**ClO_4 in EtOH for 24 h followed by washing with EtOH and drying. To analyze the so modified Au surfaces we used four complementary surface sensitive analytical techniques (contact angle measurements, atomic-force microscopy (AFM), X-ray photoelectron spectroscopy (XPS), and spectroscopic ellipsometry).[71]

Contact angles and atomic-force microscopy: The immobilization of **2**ClO_4 to gold was expected to change the wettability and roughness of the surface. Therefore, the immobilization of the complexes was probed by static water contact angle measurements and AFM topography analysis. Table 1 lists the results.

Table 1. Water contact angles and rms roughness data obtained for gold films modified with various dinickel(II) complexes.

Entry	Compound	Contact angle [°][a]	rms roughness [nm]
1	bare gold (EtOH)	75.8 (1.5)	0.6 (1)
2	$PPh_2(C_6H_4$-4-$CO_2H)$	74.9 (1.4)	n.d.[b]
3	$[Ni_2L(dppba)]ClO_4$ (**2**ClO_4)	71.5 (1.6)	1.7 (5)
4	$[Ni_2L(dppba)]BPh_4$ (**2**BPh_4)	76.7 (1.9)	1.6 (2)
5	$[Ni_2L(dppba)]ClO_4$ (**2**ClO_4) (after washing with $NaBPh_4$)	76.5 (2.1)	n.d.[b]
6	$[Ni_2L(O_2CPh)]ClO_4$	75.9 (2.0)	0.6
7	$[Ni_2L(OAc)]BPh_4$	75.8 (1.5)	0.6

[a] The values represent the average of ten 4 μL drops of destilled, deionized water. Standard deviations are given in parentheses. The "bare" gold surfaces were identically treated to the modified surfaces except with omission of any adsorbate in the solvent. [b] n.d. = not determined.

The contact angle measurements showed small but significant variations, indicating that the complexes bind indeed to the gold surface. For the unmodified gold-containing adventitious, nonpolar material a contact angle of 75.8° was obtained, which agrees with the value reported in the literature.[72] Very little is known about water contact angle of tertiary phosphines on the coinage metals.[35,36,73,74] The contact angle of the free Hdppba ligand has not been reported previously.[75] The value of 74.9° is relatively high for a carboxylate terminated monolayer, suggesting that the CO_2H groups are involved in intermolecular H-bonding interactions. Indeed, such an effect is known to increase the hydrophobicity of rather polar molecules.[76] Upon immobilization of the $[Ni_2L(dppba)]ClO_4$ complex salt, the contact angle reduces slightly relative to the unmodified gold, indicating a surface transition to a more hydrophilic state. This is not surprising given the salt-like character of the adsorbates. The contact angle for immobilized **2**ClO_4 on gold (Table 1, entry 3) is comparable with those of alkane thiol monolayers terminated with ester, alkoxy, or thioester groups.[77] The angle seems to be quite high for an ionic compound, but given that the charges are well-shielded by the apolar groups of the macrocyclic ligands, this is not surprising. A thin film of the more lipophilic tetraphenylborate salt **2**BPh_4 on gold increases the contact angle by 5.2° (Table 1, entry 4), which could be expected since the BPh_4^- group is more hydrophobic than the ClO_4^- ion. The contact angle measurements also revealed that complexes such as $[Ni_2L(O_2CPh)]BPh_4$ and $[Ni_2L(OAc)]ClO_4$, which lack end groups for surface fixation, are not chemisorbed on the gold surfaces (Table 1, entries 6 and 7). It is also interesting to note that the physisorbed anions of the immobilized salts can be exchanged for one another by surface metathesis reactions. The chemisorbed cationic complexes remain attached on the surfaces. Thus $[Ni_2L(dppba)]ClO_4$ on gold when treated with $NaBPh_4$ undergoes an anion exchange reaction to produce $[Ni_2L(dppba)]BPh_4$ (Table 1, entry 5). Such anion exchange reactions were observed by others, for example, for polycations attached to solid surfaces.[78]

The trend observed with the contact angle measurements is also reflected in the values of the root mean squared (rms) roughness determined by using AFM. Figure 10 shows

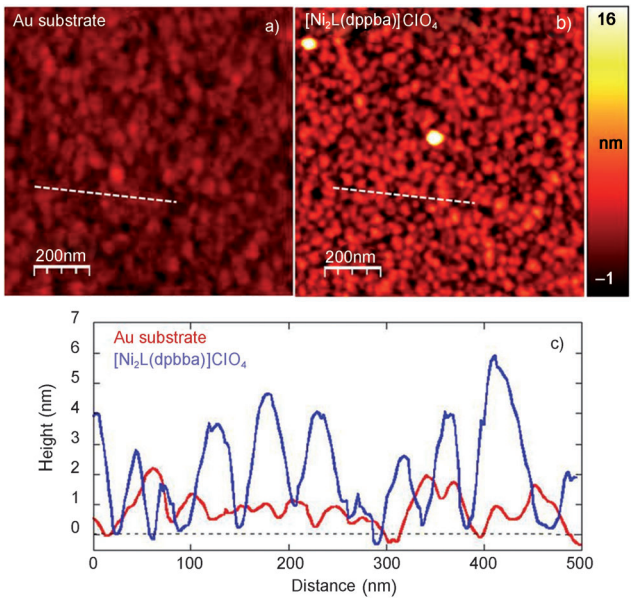

Figure 10. AFM topography characteristics considering a 1×1 μm² area, a) Au substrate as grown with a roughness of 0.6(1) nm (rms), b) Au substrate after deposition of $[Ni_2L(dppba)]ClO_4$ with a roughness of 1.7(5) nm (rms), c) AFM profile following the white-dotted lines in (a) and (b).

a comparison between the topography of $[Ni_2L(dppba)]ClO_4$ (**2**ClO_4) and of the uncovered Au substrate along with the comparison of two line profiles. As can be seen, the rms roughness of $[Ni_2L(dppba)]ClO_4$ on gold is by 10 Å larger than that of the pure gold substrate. In addition, the rms roughnesses of the $[Ni_2L(O_2CMe)]ClO_4$ and $[Ni_2L(O_2CPh)]ClO_4$ compounds (Table 1, entries 6 and 7) had similar rms values as the substrate.

XPS studies: The attachment of $[Ni_2L(dppba)]ClO_4$ (**2**ClO_4) to the gold surface was further analyzed by X-ray photoelec-

tron spectroscopy (XPS).[69] XPS spectra were recorded for bulk **2**ClO_4 and for a freshly prepared sample of **2**ClO_4 chemisorbed on gold. Photoelectron peaks of Ni, P, S, Cl, C, and O were observed. However, the long exposure time led to significant X-ray-induced damage, which particularly affected the ClO_4^- groups, the bridging thiolate sulfur atoms of the N_6S_2 macrocycle, and the P atoms as further detailed below.[79] Table 2 lists the selected peak positions and their assignments.

Table 2. XPS binding energies (eV) for **2**ClO_4 and for **2**ClO_4 chemisorbed on gold.[a]

Element	Bulk **2**ClO_4[b]	**2**ClO_4 on Au(111)[c]	Assignment
P($2p_{3/2}$)	132.2	131.1	R_3P
P($2p_{1/2}$)	133.2	132.1	
Relative intensity [%]	33	39	
P($2p_{3/2}$)	134.1	133.4	R_3PO, (or $P(OR)_3$)
P($2p_{1/2}$)	135.1	134.4	
Relative intensity [%]	49	61	
P($2p_{3/2}$)	139.9	n.o.[d]	PO_4^{3-}
P($2p_{1/2}$)	140.9	n.o.[d]	
Relative intensity [%]	18		
Ni($2p_{3/2}$)	856.5	856.8	Ni^{2+}
	861.7	862.1	"satellite"
	865.6	866.0	"satellite"
Ni($2p_{1/2}$) (main peak)	873.4	874.0	Ni^{2+}
	878.2	878.6	"satellite"
	882.7	883.0	"satellite"
S($2p_{3/2}$)	163.7	162.3	Ni–μSR–Ni
S($2p_{1/2}$)	164.7	163.3	
Total intensity [%]	100	50	
S($2p_{3/2}$)	169.8[b]	169.7	Ni–μSO_3R–Ni
S($2p_{1/2}$)	170.8[b]	170.7	
Total intensity [%]	traces	50	
Cl($2p_{3/2}$)	209	209	ClO_4^-
Cl($2p_{1/2}$)	211	211	
Total intensity [%]	60	traces	
Cl($2p_{3/2}$)	200	199.5	Cl^-
Cl($2p_{1/2}$)	202	201.5	
Total intensity [%]	40	100	
N(1s)	403	399	NR_3
O(1s)	533.5	533	RCO_2, RSO_3
C(1s)	287	284.9	CH (aliph. + arom.)
		286.1	C–S, C–P
		288.2	RCO_2^-

[a] The binding energies are referenced to Au $4f_{7/2}$ (84.0 eV). [b] Data acquisition time: 58 h (165 cycles). [c] Data acquisition time: 44 h (106 cycles), [d] n.o. = not observed.

Of particular evidence for surface Au–P single bonds are the oxygenation reactions that **2**ClO_4 undergoes in the bulk and on the gold surface. These oxidations are induced by O atoms, which stem from the decomposition of the ClO_4^- ions by the incident X-ray beams.[80] The XPS spectrum of bulk **2**ClO_4 shows two P($2p_{3/2}$) and P($2p_{1/2}$) photo peaks at binding energies typical for a phosphine group (Figure 11).[81,82] The feature at higher energies (134.1 eV) is assumed to be due to a phosphine oxide (R_3PO), which arises from X-ray-induced damage. The oxidation of physisorbed PR_3 ligands to R_3PO ligands was observed previously.[83] For chemisorbed **2**ClO_4 on gold, again two P($2p_{3/2}$) and

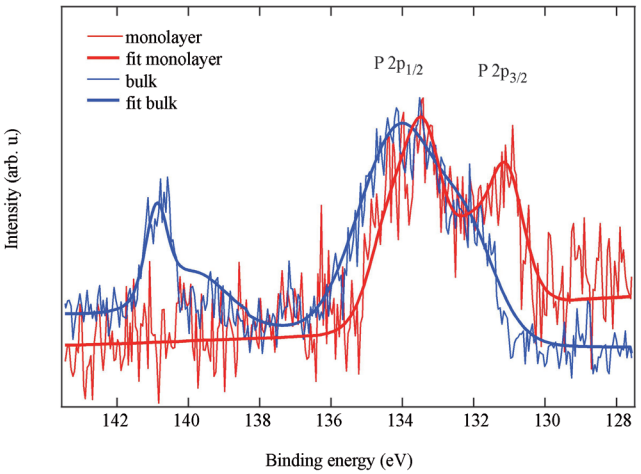

Figure 11. XPS P($2p_{3/2}$) and P($2p_{1/2}$) peaks for bulk **2**ClO_4 and for a monolayer of **2**ClO_4 on gold.

P($2p_{1/2}$) photo peaks are observed. Upon binding to Au the peak for the phosphine group is shifted to 131.1 eV, clearly showing the chemisorption of the $[Ni_2L(dppba)]^+$ complexes to the Au surface. The peak at 133.4 is attributed to X-ray induced-damage. Notice that this value is different from that of bulk **2**ClO_4. This suggests the formation of a different oxygenated species, perhaps a phosphite group ($P(OR)_3$). The incorporation of O atoms into the P–C bonds (rather than the Au–P) would be consistent with the presence of the Au–P bonds. This finding is also in excellent agreement with the previous knowledge that the P donor in the $[Ni_2L(dppba)AuPh]^+$ complex is much more resistant towards oxidation than in the parent $[Ni_2L(dppba)]^+$ complex with the free -PPh_2 group (see above). Notice that binding of the phosphine to the gold surface shifts the P($2p_{1/2}$) peaks only slightly. This specific behavior has been observed by others for R_3P ligands.[84]

The photoelectron peaks in the Ni($2p_{3/2}$) region for bulk **2**ClO_4 and for chemisorbed **2**ClO_4 on gold with the well-known satellites at 862.5 and 863 eV are characteristic of divalent, six-coordinate nickel complexes (Figure 12). These data imply that complex **2**ClO_4 undergoes no redox changes upon surface fixation.[85–88] However, the Cl(2p) regions show, besides the presence of ClO_4^- ions (209 eV), additional spectral features corresponding to chloride ions (see the Supporting Information). The observed behavior is the result of photoinduced decomposition of ClO_4^- ion into Cl^- and was reported previously.[76] A similar photoinduced conversion of the Ni-bound RS^- to RSO_3^- moieties can be observed for chemisorbed **2**ClO_4. The O atoms most likely stem again from the decomposition of the ClO_4^- ions. It is interesting that these O atoms oxidize the P atoms in bulk **2**ClO_4 and the RS^- groups in chemisorbed **2**ClO_4. This can be taken as additional evidence for the formation of an Au–P bond between molecules of **2** and the gold surface. As mentioned before, the coordination of a PR_3 ligand to a gold atom increases its stability towards oxidation, and the

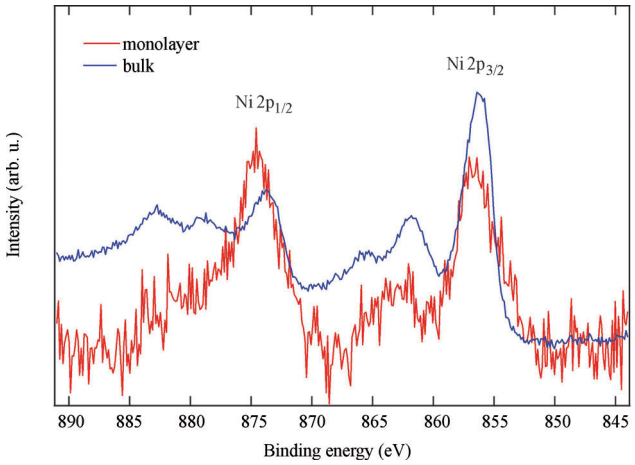

Figure 12. XPS Ni($2p_{3/2}$) peaks for bulk **2**ClO_4 and for a monolayer of **2**ClO_4 on gold.

same applies here as well. The absence of signals for free phosphine groups also rules out the presence of overlayers.

Photoelectron peaks of C, O, and Cl are also observed (the Supporting Information). The C(1 s) spectrum can be deconvoluted to three signals. The strong C(1s) signal at 284.9 eV can be attributed to the aliphatic and aromatic (CH) carbon atoms of the dppba ligand and the N_6S_2 macrocycle. The shoulder at 286.1 eV is attributed to the five electron-deficient carbon atoms bonded to electronegative sulfur and phosphorus atoms.[89] There is also a weak peak at 288.2 eV which can be attributed to the carboxylate function.[90] Taken together, the XPS spectrum provides strong evidence for a covalent Au-P linkage between **2** and the Au surface in a monolayer.

Optical thicknesses:To probe the thickness of the films spectroscopic ellipsometry measurements were carried out for a monolayer of complex **2**ClO_4 on gold, the tetraphenylborate salt **2**BPh_4, and the free phosphine Hdppba. The ellipsometry data were analyzed by using the Cauchy formula [Eq. (7)] for thin monolayers,[91] in which three parameters define the wavelength-dependent refractive index.

$$n(\lambda) = A + \frac{B}{\lambda^2} + \frac{C}{\lambda^4} \qquad (7)$$

The parameter A strongly correlates with the film thickness d, which means that fitting both A and d at the same time is not reasonable. Therefore A was kept constant at the value of 1.45, which is commonly used for the refractive index of monolayers described as transparent media.[92,93] By using this model, reasonable fits were produced resulting in average thicknesses of (4.8±4) Å for Hdppba, (16.3±7) Å for **2**ClO_4, and (15.1±8) Å for **2**BPh_4. The observed layer thickness of the Hdppba ligand is somewhat smaller than the calculated molecule size of approximately 7 Å assuming that the molecules are oriented with their pseudo-threefold axis perpendicular to the surface and that the average C-P-C angle is 105°. This deviation from the expected thickness value of one monolayer most likely arises from the relatively high film roughness of the gold substrates used rather than from an ordering by intermolecular hydrogen-bonding interactions between the adsorbate molecules. The strong dependence of film thicknesses on the film roughness was also observed by others.[94]

Nevertheless, the observed film thicknesses observed for the perchlorate and tetraphenylborate salts are in good agreement with the molecule size of ≈15 Å for the $[Ni_2L(O_2CC_6H_4PPh_2)]^+$ cation in **2**ClO_4 and **2**BPh_4 (on the basis of the corresponding atomic distances in the crystal structure of **2**ClO_4). Interestingly, the thicknesses of the layers of the perchlorate and tetraphenylborate salts are almost identical suggesting that the ClO_4^- and BPh_4^- ions are located beneath the $[Ni_2L(dppba)]^+$ moieties rather than above them in a second layer. Therefore, the ellipsometric data further support the assumption that both **2**ClO_4 and **2**BPh_4 form monolayers rather than multilayer films, with the cationic $[Ni_2L(dppba)]^+$ molecules oriented perpendicular to the Au surface.

Surface-binding model: If it can be assumed that the observed Au–P bonding interactions in **4**BPh_4 are maintained in chemisorbed $[Ni_2L(dppba)]ClO_4$ on gold, one can propose a hypothetical surface structure. Figure 13 shows a likely orientation of **2**ClO_4 on the gold surface. The height of the $[Ni_2L(dppba)]^+$ complex on the surface in this case is given by the distance between two opposing NMe substituents, which amounts to approximately 12.3 Å. In an alternate orientation (not shown in Figure 12) the $[Ni_2L]^{2+}$ fragment is rotated by 90° around the $O_2CC_6H_4$–PPh_2 bond. In this case, the height is given by two opposing *tert*-butyl CH_3 groups, which amounts to 15.5 Å (H32a···H37b).[95] This value is in reasonable agreement with the thickness determined by ellipsometry. Irrespective of the actual orientation of the $[LNi_2]^{2+}$ fragment, the surface complex presumably is also stabilized by van der Waals interactions between the Au surface and the methylene or methyl groups of the supporting macrocycle. The thiolate sulfur atoms, however, are out of range of bonding interactions with the Au surface.

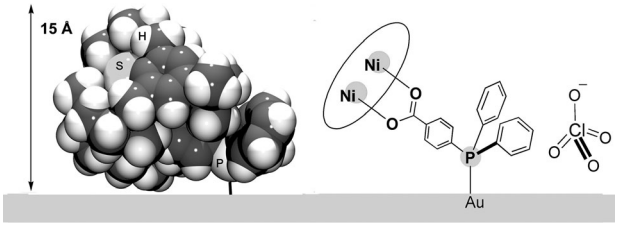

Figure 13. Proposed binding mode of **2**ClO_4 to gold (left: van der Waals representation of the cation **2**; right: representation with a Lewis formula. The macrocycle is shown as an ellipse encircling the two Ni^{2+} ions for clarity).

Conclusion

The main findings of the present work can be summarized as follows: 1) The dinuclear Ni^{II} complex $[Ni_2L(O_2CC_6H_4PPh_2)]^+$ supported by a macrocyclic hexaza-dithiophenolate ligand is readily prepared and can be isolated as the air-sensitive perchlorate $[Ni_2L(dppba)]ClO_4$ (**2**ClO_4) or tetraphenylborate $[Ni_2L(dppba)]BPh_4$ (**2**BPh_4) salt. 2) The X-ray structure determination showed that the ambidentate 4-(diphenylphosphino)benzoate co-ligand binds specifically, through its carboxylate function, to the $[Ni_2L]^{2+}$ fragment such that the soft phosphorus atom is positioned in the periphery of the complex. 3) The mode of auration of **2**ClO_4 with AuCl demonstrates that **2**ClO_4 exhibits only one gold binding site. Only the phosphine group in **2**ClO_4 is aurated. The two thiolate sulfur atoms in **2**ClO_4 exhibit no aurophilicity. 4) The $[Ni^{II}{}_2L(dppba)]^+$ complexes exhibit an $S=2$ ground state that is attained by ferromagnetic coupling of the two Ni^{II} ($S_i=1$) ions. HF-ESR measurements yield a negative axial magnetic anisotropy ($D<0$), which implies a bistable (easy axis) magnetic ground state. 5) The $[Ni_2L(dppba)]^+$ complex is redox-active and is also accessible in a mixed-valent $Ni^{II}Ni^{III}$ form of a different $S=3/2$ ground spin state. 6) Complexes of **2**ClO_4 can be chemisorbed on gold surfaces through the formation of Au–P surface bonds as clearly established by contact angle measurements, AFM spectroscopy, XPS spectroscopy, and spectroscopic ellipsometry. Finally, 7) the complexes do not change their oxidation state upon surface fixation. It would be interesting to see whether the oxidation state of **2**ClO_4 (and hence the spin state) can be switched by the tip of a scanning tunneling microscope. Such studies are underway.

Experimental Section

Materials and methods: All reagents were purchased from commercial sources unless otherwise specified. Compound $[Ni_2L(Cl)]ClO_4$ (**1**ClO_4) was prepared as described in the literature.[45] 4-(diphenylphosphane)-benzoic acid was prepared by using a fluoride-catalyzed reaction from 4-fluoroethylbenzoate and diphenyl(trimethylsilyl)phosphine.[96] Ethanol was deoxygenated with nitrogen before use. Acetonitrile was distilled from calcium hydride. The syntheses of the metal complexes were carried out under a protective atmosphere of argon. Melting points were determined in open glass capillaries and are uncorrected. The infrared spectra were recorded as KBr discs by using a Bruker Tensor 27 FT-IR spectrophotometer. Electronic absorption spectra were recorded on a Jasco V-670 UV/Vis/near-IR spectrophotometer. Elemental analysis was carried out on a VARIO EL–elemental analyzer. ESI mass spectra were recorded on a Bruker Daltronics ESQUIRE3000 PLUS spectrometer. Cyclic voltammetry measurements were carried out at 25 °C with an EG&G Princeton Applied Research potentiostat/galvanostat model 263 A. Cobaltocenium hexafluorophosphate (Cp_2CoPF_6) was used as an internal standard. All potentials are given versus SCE but are standardized against the ferrocenium/ferrocene couple.[97] Temperature-dependent magnetic susceptibility measurements on powdered solid samples were carried out by using a MPMS 7XL SQUID magnetometer (Quantum Design) over a temperature range 2–330 K at an applied magnetic field of 0.5 Tesla. The observed susceptibility data were corrected for underlying diamagnetism. CAUTION! Perchlorate salts of transition-metal complexes are hazardous and may explode. Only small quantities should be prepared and great care should be taken.

$[Ni_2L(dppba)]ClO_4$ (2ClO_4): A solution of Hdppba (50 mg, 0.163 mmol) in MeOH was added to a solution of $[Ni_2L(\mu\text{-}Cl)]ClO_4$ (100 mg, 0.108 mmol) in MeOH (25 mL). Triethylamine (16.2 mg, 0.16 mmol) was then added and the ocher-colored suspension turned into a clear-green solution, which was stirred for 48 h at RT. A solution of $LiClO_4{\cdot}3H_2O$ (87.1 mg. 0.54 mmol) in EtOH (20 mL) was added, and stirring was continued for 30 min. The mixture was concentrated (rotary evaporator) to ≈25 mL. The green, microcrystalline precipitate was filtered, washed with EtOH and Et_2O. Yield: 111 mg (86 %). M.p. 320–324 °C (decomp.); IR (KBr pellet): $\tilde{\nu}=3443$ (w), 2961 (m), 2867 (m), 1599 (s), 1550 (m, ν_{as} (RCO_2^-)), 1461 (s), 1408 (s, ν_s (RCO_2^-)), 1363 (m), 1309 (w), 1265 (w), 1233 (w), 1201 (w), 1152 (w), 1092 (vs, ClO_4^-), 1040 (m), 931 (w), 913 (m), 881 (w), 825 (m), 817 (m), 768 (m), 746 (w), 719 (w), 699 (m), 623 (m, ClO_4^-), 495 cm^{-1} (w); UV/Vis (CH_2Cl_2): λ_{max} (ε) = 227 (48400), 272 (15000), 334 (11800), 385 (2100), 650 (34), 1122 nm (68 $M^{-1}cm^{-1}$); MS (ESI): *m/z* (CH_3CN) = 1089.4 $[M-ClO_4]^+$; elemental analysis calcd (%) for $C_{57}H_{78}ClN_6Ni_2O_6PS_2$ (1191.21): C 57.47, H 6.60, N 7.06, S 5.38; found: C 57.25, H 6.39, N 6.97, S 5.27. The tetraphenylborate salt **2**BPh_4 was prepared by adding a solution of $NaBPh_4$ (14.4 mg, 42.0 μmol) in EtOH (10 mL) to a solution of **2**ClO_4 (10.0 mg, 8.39 μmol) in CH_2Cl_2 (10 mL). Yield: 11.5 mg (97 %). IR (KBr pellet): $\tilde{\nu}=3424$ (vw), 3052 (m), 3033 (m), 2961 (m), 2925 (m), 2839 (m), 1589 (s), 1548 (w), 1479 (m), 1458 (s), 1420 (vs), 1394 (m), 1363 (m), 1308 (w), 1264 (m), 1231 (w), 1199 (vw), 1181 (vw), 1150 (w), 1133 (w), 1075 (m), 1058 (m), 1039 (m), 1001 (w), 929 (w), 912 (m), 879 (m), 844 (m), 823 (m), 777 (vw), 748 (m), 733 (m), 703 (vs), 629 (w), 611 (m), 562 (w), 536 (w), 486 cm^{-1} (m).

$[Ni_2L(dppba)AuCl]ClO_4$ (3ClO_4): A green-colored solution of $[Ni_2L(dppba)]ClO_4$ (100 mg, 83.4 μmol) in CH_2Cl_2 (15 mL) was added through a dropping funnel over a 30 min period to an ocher-colored suspension of AuCl (19.5 mg, 80.0 μmol) in CH_2Cl_2 (15 mL). The resulting green solution was stirred for an additional 24 h at ambient temperature, filtered, and the filtrate combined with a solution of $LiClO_4{\cdot}3H_2O$ (67.3 mg, 0.42 mmol) in EtOH. After stirring for a further 30 min, the CH_2Cl_2 was removed by rotary evaporation to give the product as a green solid, which was filtered and washed with cold EtOH and Et_2O. Yield: 108 mg (91 % based on $[Ni_2L(dppba)]ClO_4$). M.p. 268–270 °C (decomposes without melting.); IR (KBr pellet): $\tilde{\nu}=$ 3447 (w), 2953 (m), 2864 (m), 1602 (s), 1553 (m, ν_{as} (RCO_2^-)), 1461 (s), 1438 (m, ν_s (RCO_2^-)), 1398 (s), 1363 (m), 1308 (w), 1265 (w), 1233 (w), 1200 (vw), 1153 (w), 1097 (vs, ClO_4^-), 1039 (m), 999 (w), 930 (w), 912 (w), 881 (w), 825 (m), 768 (w), 752 (w), 726 (m), 694 (m), 623 (m, ClO_4^-), 564 (w), 534 (w), 490 (w), 415 cm^{-1} (w); UV/Vis (CH_2Cl_2): λ_{max} (ε) = 231 (47700), 304 (13400), 334 (9900), 381 (1900), 652 (35), 1119 nm (70 $M^{-1}cm^{-1}$); MS (ESI): *m/z* (CH_3CN) = 1321.4 $[M-ClO_4]^+$; elemental analysis calcd (%) for $C_{57}H_{78}AuCl_2N_6Ni_2O_6PS_2$ (1423.63): C 48.09; H 5.52, N 5.90, S 4.50; found: C 48.09, H 5.64, N 5.59, S 4.63.

$[Ni_2L(dppba)AuPh]BPh_4$ (4BPh_4): A solution of $NaBPh_4$ (120 mg, 350 μmol) in EtOH (10 mL) was added to a solution of $[Ni_2L(dppba)AuCl]ClO_4$ (100 mg, 70.24 μmol) in CH_2Cl_2 (15 mL). The mixture was stirred for 1 h, when CH_2Cl_2 was removed under reduced pressure. The resulting green solid was isolated by filtration, washed with cold EtOH and Et_2O. Yield: 93 % (based on $[Ni_2L(dppba)AuCl]ClO_4$). The crude product was purified by recrystallization from a mixed CH_2Cl_2/$CHCl_3$/*n*-hexanes solvent system. M.p. 263–265 °C (decomposes without melting.); IR (KBr pellet): $\tilde{\nu}=3444$ (w), 3052 (m), 3049 (w), 2962 (m), 2857 (m), 1600 (s), 1552 (m, ν_{as} (RCO_2^-)), 1460 (vs), 1437 (m, ν_s (RCO_2^-)), 1395 (s), 1263 (m), 1307 (w), 1265 (w), 1232 (w), 1151 (w), 1099 (w), 1076 (m), 1057 (m), 1041 (m), 999 (w), 930 (w), 912 (w), 881 (w), 825 (m), 768 (w), 728 (s), 703 (vs, BPh_4^-), 631 (m), 612 (m), 525 cm^{-1} (m); UV/Vis (CH_2Cl_2): λ_{max} (ε) = 229 (68100), 306 (11300), 334 (8000), 387 (1300), 651 (33), 1119 nm (68 $M^{-1}cm^{-1}$); MS (ESI): *m/z* (CH_3CN) = 1363.3 $[M-BPh_4]^+$; elemental analysis calcd (%) for $C_{87}H_{103}AuBN_6Ni_2O_2PS_2$ (1685.06): C 62.01; H 6.16; N 4.99; S 3.81; found: C 61.95; H 6.08; N 4.98; S 3.82.

Preparation of gold substrates: Substrates were prepared by magnetron sputtering of 100 nm Au onto polished silicon wafers Si(111), pre-coated

with a 20 nm thick adhesion layer of titanium. The root mean square roughness of the gold substrates was ≤ 0.6 nm (by using AFM). The substrates were cut into pieces (1 cm × 1 cm), cleaned by ultrasonic treatment in piranha solution (H_2SO_4/H_2O_2, 3:1; CAUTION! piranha solution reacts violently with organic materials),[19,98] followed by washing with dichloromethane, ethanol, and deionized water.

Contact angles: Surface hydrophobicity was examined by performing water contact angle measurements (Sessile Drop Method) with a DSA II (Krüss, Hamburg, Germany) contact angle analyzer. The contact angle measurements were collected by using a 4 μL drop size of deionized, distilled water. At least 10 contact angles per five different locations were averaged. The spectra were analyzed according to Owens-Wendt-Rabel-Kaelble.

Atomic-force microscopy: Topography data were acquired with an Agilent 5600 LS AFM system, under Argon (Ar)-controlled environmental conditions to maintain the integrity of the organic system. Measurements were performed in tapping mode to minimize the contact between the AFM probe and the sample surface and avoid damage or modification of the topographic characteristics. Special ultra-sharp (4–10 nm tip radius) Olympus cantilevers were employed allowing high sensitivity measurements. Data shown in the respective Figure 10 correspond to an area of $1 \times 1\ \mu m^2$, although a mapping of the topographic characteristics was performed on different points of the samples to verify the uniformity of the organic system over the Au substrate.

Ellipsometry: A M-2000 T-Solar ellipsometer (J. A. Woollam Co., Inc.) operating with a Xe lamp was employed for ellipsometric measurements in the spectral range from 0.7 to 5 eV. The cleaned gold substrates were immersed in a 1×10^{-3} M solution of the complexes in dichloromethane for at least 12 h, after which they were rinsed with absolute ethanol, blown dry with ultrahigh purity nitrogen, and immediately measured under ambient conditions. The reported thickness values represent the average of at least nine measurements at different locations on the surface of the sample at three different incident angles (65, 70, and 75°). Every sample series evaluated by spectroscopic ellipsometry consists of 3 to 5 samples of the same molecular complex produced under the same experimental conditions. The error bars represent the standard deviation from the mean thickness value within one sample series. The scatter observed in the data was typically ±0.6 nm, arising most likely from a film roughness of the gold substrates of about 0.8 nm (measured by AFM).

The data analysis was performed with the CompleteEASE software from the J. A. Woollam Company.[99] The model used for the thickness determination consists of two layers, whereby the first one is the gold substrate and the second one is a Cauchy layer. As the theory describing this layer is applicable only for non-absorbing films, one usually has to restrict the evaluated energy range to an appropriate spectral region. Because of the small layer thickness the absorption was small enough to use the data of the entire energy range from 0.7 to 5.0 eV.

X-ray photoelectron spectroscopy: XPS spectra were obtained on a commercial PHI 5600 spectrometer equipped with two light sources. A monochromatized $Al_{K\alpha}$ source provided photons with an energy of 1486.6 eV, which was used for the core level studies. The total energy resolution was 350 meV. The gold foils (Au, purity 99.59%) were cleaned in a ultrasonic bath. The substrate was immersed in a 1×10^{-3} M solution of **2**ClO_4 in dichloromethane for at least 12 h, washed with dichloromethane, then ethanol, and immediately transferred into the spectrometer. Energy referencing was based on the Au $4f_{7/2}$ peak at 84.0 eV. All samples were studied at room temperature at a pressure of approximately 2×10^{-10} mbar. Spectra were analyzed using CasaXPS.[100]

Crystallography: Single crystals of **2**BPh_4 suitable for X-ray crystallography were obtained by recrystallization from MeCN/EtOH. Single crystals of **4**$BPh_4 \cdot 1.5CH_2Cl_2 \cdot 0.5CHCl_3 \cdot 0.5H_2O$ were obtained by slow evaporation of a mixed $CHCl_3$, CH_2Cl_2, hexanes (1:1:1, v/v/v) solution. The diffraction experiments were carried out at 203 K on a STOE IPDS-2T X-ray diffractometer. The intensity data were processed with the program STOE X-AREA.[101] Structures were solved by direct methods[102] and refined by full-matrix least-squares on the basis of all data against F^2 by using SHELXL-97.[103] PLATON was used to search for higher symmetry.[104] H atoms were placed in calculated positions and treated isotropically by using the 1.2-fold U_{iso} value of the parent atom except methyl protons, which were assigned the 1.5-fold U_{iso} value of the parent C atoms. Unless otherwise noted, all non-hydrogen atoms were refined anisotropically. ORTEP-3 was used for the artwork of the structures.[105]

In the crystal structure of **4**$BPh_4 \cdot 1.5CH_2Cl_2 \cdot 0.5CHCl_3 \cdot 0.5H_2O$, one *t*Bu group of one of the two crystallographically independent molecules was found to be disordered over two positions. A split atom model with restrained C–C and C···C distances was applied by using SADI instructions implemented in SHELXTL. The site occupancies of the respective orientations were refined as follows: C(32a)C(33a)C(34a)/C(32b)C(33b)C(34b) = 0.60:0.40. The C and Cl atoms of one CH_2Cl_2 solvate molecule were refined isotropically.

CCDC-910079 ([Ni_2L(dppba)]BPh_4) and CCDC-910080 ([Ni_2L(dppba)AuPh)]$BPh_4 \cdot 1.5CH_2Cl_2 \cdot 0.5CHCl_3 \cdot 0.5H_2O$) contain the supplementary crystallographic data for this paper. These data can be obtained free of charge from The Cambridge Crystallographic Data Centre via www.ccdc.cam.ac.uk/data_request/cif.

Crystallographic data for [Ni_2L(dppba)]BPh_4: $C_{81}H_{98}BN_6Ni_2O_2PS_2$, $M_w = 1410.97$, triclinic, space group $P\bar{1}$, $a = 11.033(2)$, $b = 17.813(4)$, $c = 19.616(4)$ Å, $\alpha = 100.48(3)$, $\beta = 104.44(3)$, $\gamma = 98.58(3)$°, $V = 3593.6(12)$ Å^3, $Z = 2$, $\rho_{calcd} = 1.304$ g cm^{-3}, $\mu(Mo_{K\alpha}) = 0.656$ mm^{-1}, crystal size $0.30 \times 0.25 \times 0.20$ mm, θ limits: 1.42–27.39°. $T = 183$ K. Of 29738 measured reflections ($R_{int} = 0.094$), 15471 were unique and 8558 observed ($I > 2\sigma(I)$). Refinement converged to $R_1 = 0.0649$, $wR_2 = 0.1507$ (for observed data), $R_1 = 0.1236$, $wR_2 = 0.1537$ for all data. Max, min peaks: 0.990, −0.879 e Å^3.

Crystallographic data for [Ni_2L(dppba)AuPh)]$BPh_4 \cdot 1.5CH_2Cl_2 \cdot 0.5CHCl_3 \cdot 0.5H_2O$: $C_{89}H_{107.50}AuBCl_{4.50}N_6Ni_2O_{2.50}PS_2$, $M_w = 1881.12$, monoclinic, space group $P2_1/n$, $a = 14.159(3)$, $b = 37.431(8)$, $c = 32.374(7)$ Å, $\beta = 93.17(3)$°, $V = 17131(6)$ Å^3, $Z = 8$, $\rho_{calcd} = 1.459$ g cm^{-3}, $\mu(Mo_{K\alpha}) = 2.403$ mm^{-1}, crystal size $0.25 \times 0.20 \times 0.20$ mm, θ limits: 1.42–27.39°. $T = 181(2)$ K. Of 166354 measured reflections ($R_{int} = 0.11$), 43106 were unique and 24877 observed ($I > 2\sigma(I)$). Refinement converged to $R_1 = 0.0522$, $wR_2 = 0.1283$ (for observed data), $R_1 = 0.0993$, $wR_2 = 0.1428$ for all data. Max, min peaks: 1.937, −1.878 e Å^3.

Acknowledgements

This work was supported by the Deutsche Forschungsgemeinschaft DFG FOR 1154 "Towards molecular spintronics" and the University of Leipzig. J. Lach thanks the Sächsische Aufbaubank (SAB) for an ESF grant (Europäischer Sozialfonds).

[1] For reviews on the organization of a magnetically bistable molecule on surfaces, see: a) A. Cornia, M. Mannini, P. Sainctavit, R. Sessoli, *Chem. Soc. Rev.* **2011**, *40*, 3076–3091; b) J. Gómez-Segura, J. Veciana, D. Ruiz-Molina, *Chem. Commun.* **2007**, 3699–3707; c) M. Cavallini, M. Facchini, C. Albonetti, F. Biscarini, *Phys. Chem. Chem. Phys.* **2008**, *10*, 784–793.

[2] For reviews for integration of electronically bistable molecule or molecular switches in thin film devices, see: a) K. Szaciłowski, *Chem. Rev.* **2008**, *108*, 3481–3548; b) V. A. Dediu, L. E. Hueso, I. Bergenti, C. Taliani, *Nat. Mater.* **2009**, *8*, 707–716; c) M. Wohlgenannt, *Phys. Status Solidi RRL* **2012**, *6*, 229–242.

[3] D. Gatteschi, R. Sessoli, J. Villain, *Molecular Nanomagnets*, Oxford University Press, Oxford, **2006**.

[4] F. Troiania, M. Affronte, *Chem. Soc. Rev.* **2011**, *40*, 3119–3129.

[5] J. M. Seminario, *Nat. Mater.* **2005**, *4*, 111–113.

[6] A. R. Rocha, V. M. García-Suárez, S. W. Bailey, C. J. Lambert, J. Ferrer, S. Sanvito, *Nat. Mater.* **2005**, *4*, 335–339.

[7] L. Bogani, W. Wernsdorfer, *Nat. Mater.* **2008**, *7*, 179–186.

[8] V. Meded, A. Bagrets, K. Fink, R. Chandrasekar, M. Ruben, F. Evers, A. Bernand-Mantel, J. S. Seldenthuis, A. Beukman, H. S. J. van der Zant, *Phys. Rev. B* **2011**, *83*, 245415–1–13.

[9] F. Prins, M. Monrabal-Capilla, E. A. Osorio, E. Coronado, H. S. J. van der Zant, *Adv. Mater.* **2011**, *23*, 1545–1549.

[10] S. Shi, G. Schmerber, J. Arabski, J.-B. Beaufrand, D. J. Kim, S. Boukari, M. Bowen, N. T. Kemp, N. Viart, G. Rogez, E. Beaurepaire, H. Aubriet, J. Petersen, C. Becker, D. Ruch, *Appl. Phys. Lett.* **2009**, *95*, 043303–1–3.

[11] For thin films of phthalocyanines, see a) D. E. Barlow, L. Scudiero, K. W. Hipps, *Langmuir* **2004**, *20*, 4413–4421; b) C. Iacovita, M. V. Iacovita, B. W. Heinrich, T. Brumme, J. Kortus, L. Limot, J. P. Bucher, *Phys. Rev. Lett.* **2008**, *101*, 116602–1–4; c) C. Wäckerlin, D. Chylarecka, A. Kleibert, K. Müller, C. Iacovita, F. Nolting, T. A. Jung, N. Ballav, *Nat. Commun.* **2010**, *1*, 1–7; d) M. Schmid, A. Kaftan, H.-P. Steinrück, J. M. Gottfried, *Surface Science* **2012**, *606*, 945–949; e) M. Toader, M. Knupfer, D. R. T. Zahn, M. Hietschold, *Surface Science* **2011**, *605*, 1507–1512; f) S. Lindner, M. Knupfer, R. Friedrich, T. Hahn, J. Kortus, *Phys. Rev. Lett.* **2012**, *109*, 027601.

[12] For thin films of metallo-porphyrines, see: a) A. Scheybal, T. Ramsvik, R. Bertschinger, M. Putero, F. Nolting, T. A. Jung, *Chem. Phys. Lett.* **2005**, *411*, 214–220; b) H. Wende, M. Bernien, J. Luo, C. Sorg, N. Ponpandian, J. Kurde, J. Miguel, M. Piantek, X. Xu, P. Eckhold, W. Kuch, K. Baberschke, P. M. Panchmatia, B. Sanyal, P. M. Oppeneer, O. Eriksson, *Nat. Mater.* **2007**, *6*, 516–520; c) M. Bernien, J. Miguel, C. Weis, M. E. Ali, J. Kurde, B. Krumme, P. M. Panchmatia, B. Sanyal, M. Piantek, P. Srivastava, K. Baberschke, P. M. Oppeneer, O. Eriksson, W. Kuch, H. Wende, *Phys. Rev. Lett.* **2009**, *102*, 047202–1–4; d) P. M. Oppeneer, P. M. Panchmatia, N. Sanyal, O. Eriksson, M. E. Ali, *Prog. Surf. Sci.* **2009**, *84*, 18–29.

[13] SMM arranged in thin films or multi-layers: a) M. Clemente-León, H. Soyer, E. Coronado, C. Mingotaud, C. J. Gómez-García, P. Delhaès, *Angew. Chem.* **1998**, *110*, 3053–3056; *Angew. Chem. Int. Ed.* **1998**, *37*, 2842–2845; b) A. Cornia, A. C. Fabretti, M. Pacchioni, L. Zobbi, D. Bonacchi, A. Caneschi, D. Gatteschi, R. Biagi, U. Del Pennino, V. De Renzi, L. Gurevich, H. S. J. van Der Zant, *Angew. Chem.* **2003**, *115*, 1683–1686; *Angew. Chem. Int. Ed.* **2003**, *42*, 1645–1648.

[14] Surface SCO-compounds arranged in rows: M. S. Alam, M. Stocker, M. Gieb, K. Müller, P. Haryono, K. Student, A. Grohmann, *Angew. Chem.* **2010**, *122*, 1178–1182; *Angew. Chem. Int. Ed.* **2010**, *49*, 1159–1163.

[15] a) W. Hieringer, K. Flechtner, A. Kretschmann, K. Seufert, W. Auwärter, J. V. Barth, A. Görling, H.-P. Steinrück, J. M. Gottfried, *J. Am. Chem. Soc.* **2011**, *133*, 6206–6222; b) T. Komeda, H. Isshiki, J. Liu, Y.-F. Zhang, N. Lorente, K. Katoh, B. K. Breedlove, M. Yamashita, *Nat. Commun.* **2011**, *2*, 217–223; c) T. Choi, S. Bedwani, A. Rochefort, C.-Y. Chen, A. J. Epstein, J. A. Gupta, *Nano Lett.* **2010**, *10*, 4175–4180; d) T. G. Gopakumar, F. Matino, H. Naggert, A. Bannwarth, F. Tuczek, R. Berndt, *Angew. Chem.* **2012**, *124*, 6367–6371; *Angew. Chem. Int. Ed.* **2012**, *51*, 6262–6266.

[16] SMM's arranged in thin films: P. Gambardella, S. Stepanow, A. Dmitriev, J. Honolka, F. M. F. de Groot, M. Lingenfelder; S. S. Gupta, D. D. Sarma, P. Bencok, S. Stanescu, S. Clair, S. Pons, N. Lin, A. P. Seitsonen, H. Brune, J. V. Barth, K. Kern, *Nat. Mater.* **2009**, *8*, 189–193; S. S. Gupta, D. D. Sarma, P. Bencok, S. Stanescu, S. Clair, S. Pons, N. Lin, A. P. Seitsonen, H. Brune, J. V. Barth, K. Kern, *Nat. Mater.* **2009**, *8*, 189–193.

[17] SCO compounds arranged in thin films or multi-layers a) H. Soyer, C. Mingotaud, M.-L. Boillot, P. Delhaés, *Thin Solid Films* **1998**, *327–329*, 435–438; b) A. B. Gaspar, M. Seredyuk, P. Gütlich, *Coord. Chem. Rev.* **2009**, *253*, 2399–2413; c) G. Agustí, S. Cobo, A. B. Gaspar, G. Molnár, N. O. Moussa, P. Á. Szilágyi, V. Pálfi, C. Vieu, M. C. Muoz, J. A. Real, A. Bousseksou, *Chem. Mater.* **2008**, *20*, 6721–6732; d) I. Boldog, A. B. Gaspar, V. Martínez, P. Pardo-Ibañez, V. Ksenofontov, A. Bhattacharjee, P. Gütlich, J. A. Real, *Angew. Chem.* **2008**, *120*, 6533–6537; *Angew. Chem. Int. Ed.* **2008**, *47*, 6433–6437; e) F. Volatron, L. Catala, E. Rivière, A. Gloter, O. Stéphan, T. Mallah, *Inorg. Chem.* **2008**, *47*, 6584–6586; f) C. Rajadurai, F. Schramm, S. Brink, O. Fuhr, M. Ghafari, R. Kruk, M. Ruben, *Inorg. Chem.* **2006**, *45*, 10019–10021; g) Y. Bodenthin, U. Pietsch, H. Möhwald, D. G. Kurth, *J. Am. Chem. Soc.* **2005**, *127*, 3110–3114.

[18] L. Margheriti, M. Mannini, L. Sorace, L. Gorini, D. Gatteschi, A. Caneschi, D. Chiappe, R. Moroni, F. Buatier de Mongeot, A. Comia, F. M. Piras, A. Magnani, R. Sessoli, *Small* **2009**, *5*, 1460–1466.

[19] J. C. Love, L. A. Estroff, J. K. Kriebel, R. G. Nuzzo, G. M. Whitesides, *Chem. Rev.* **2005**, *105*, 1103–1169.

[20] A. Ulman, *Chem. Rev.* **1996**, *96*, 1533–1554.

[21] Y. Xia, G. M. Whitesides, *Angew. Chem.* **1998**, *110*, 568–594; *Angew. Chem. Int. Ed.* **1998**, *37*, 550–575.

[22] a) A. Naitabdi, J.-P. Bucher, P. Gerbier, P. Rabu, M. Drillon, *Adv. Mater.* **2005**, *17*, 1612–1616; b) J. S. Steckel, N. S. Persky, C. R. Martinez, C. L. Barnes, E. A. Fry, J. Kulkarni, J. D. Burgess, R. B. Pacheco, S. L. Stoll, *Nano Lett.* **2004**, *4*, 399–402; c) S. Voss, M. Burgert, M. Fonin, U. Groth, U. Rüdiger, *Dalton Trans.* **2008**, 499–505; d) E. Coronado, A. Forment-Aliaga, F. M. Romero, V. Corradini, R. Biagi, V. De Renzi, A. Gambardella, U. Del Pennino, *Inorg. Chem.* **2005**, *44*, 7693–7695.

[23] M. Mannini, F. Pineider, P. Sainctavit, C. Danieli, E. Otero, A. M. T. Sciancalepore, M.-A. Arrio, A. Cornia, D. Gatteschi, R. Sessoli, *Nat. Mater.* **2009**, *8*, 194–197.

[24] a) L. Zobbi, M. Mannini, M. Pacchioni, G. Chastanet, D. Bonacchi, C. Zanardi, R. Biagi, U. Del Pennino, D. Gatteschi, A. Cornia, R. Sessoli, *Chem. Commun.* **2005**, 1640–1642; b) M. Mannini, F. Pineider, C. Danieli, F. Totti, L. Sorace, P. Sainctavit, M.-A. Arrio, E. Otero, L. Joly, J. C. Cezar, A. Cornia, R. Sessoli, *Nature* **2010**, *468*, 417–421; c) M. Pacchioni, A. Cornia, A. C. Fabretti, L. Zobbi, D. Bonacchi, A. Caneschi, G. Chastanet, D. Gatteschi, R. Sessoli, *Chem. Commun.* **2004**, 2604–2605.

[25] V. Lozan, C. Loose, J. Kortus, B. Kersting, *Coord. Chem. Rev.* **2009**, *253*, 2244–2260.

[26] U. Lehmann, J. Lach, C. Loose, T. Hahn, B. Kersting, J. Kortus, *Dalton Trans.* **2013**, *42*, 987–996.

[27] V. Lozan, B. Kersting, *Inorg. Chem.* **2008**, *47*, 5386–5393.

[28] U. Lehmann, J. Klingele, V. Lozan, G. Steinfeld, M. H. Klingele, S. Käss, A. Rodenstein, B. Kersting, *Inorg. Chem.* **2010**, *49*, 11018–11029.

[29] B. Kersting in *Activating Unreactive Molecules: The Role of Secondary Interactions* (Eds.: C. Bolm, F. E. Hahn), Wiley-VCH, Weinheim **2009**, Chapter 1, pp. 1–17.

[30] B. Kersting, U. Lehmann, *Adv. Inorg. Chem.* **2009**, *61*, 407–470, (Ed.: R. v. Eldik, C. D. Hubbard)

[31] P. Chaudhuri, V. Kataev, B. Büchner, H.-H. Klauss, B. Kersting, F. Meyer, *Coord. Chem. Rev.* **2009**, *253*, 2261–2285.

[32] C. Loose, E. Ruiz, B. Kersting, J. Kortus, *Chem. Phys. Lett.* **2008**, *452*, 38–43.

[33] G. Steinfeld, V. Lozan, H.-J. Krüger, B. Kersting, *Angew. Chem.* **2009**, *121*, 1988–1991; *Angew. Chem. Int. Ed.* **2009**, *48*, 1954–1957.

[34] J. Lach, T. Hahn, B. Kersting, J. Kortus, *Eur. J. Inorg. Chem.* **2012**, 2381–2388.

[35] J. Lach, A. Jeremies, V. Lozan, C. Loose, T. Hahn, J. Kortus, B. Kersting, *Inorg. Chem.* **2012**, *51*, 12380–12391.

[36] G. Westermark, I. Persson, *Colloids Surf. A* **1998**, *144*, 149–166.

[37] U. B. Steiner, P. Neuenschwander, R. W. Caseri, U. W. Suter, *Langmuir* **1992**, *8*, 90–94.

[38] B. M. Trost, M. R. Machacek, A. Aponick, *Acc. Chem. Res.* **2006**, *39*, 747–60.

[39] G. Schmid, *Chem. Soc. Rev.* **2008**, *37*, 1909–1930.

[40] B. K. Teo, X. Shi, H. Zhang, *J. Am. Chem. Soc.* **1992**, *114*, 2743–2745.

[41] Z. Wang, L. Ma, *Coord. Chem. Rev.* **2009**, *253*, 1607–1618.

[42] J. M. Pettibone, J. W. Hudgens, *J. Phys. Chem. Lett.* **2010**, *1*, 2536–2540.

[43] P. M. Shem, R. Sardar, J. S. Shumaker-Parry, *Langmuir* **2009**, *25*, 13279–13283.

[44] J. M. Pettibone, J. W. Hudgens, *ACS Nano* **2011**, *5*, 2989–3002.

[45] Y. S. Chung, K. Evans, W. Glaunsinger, *Appl. Surf. Sci.* **1998**, *125*, 65–72.

[46] B. Kersting, G. Steinfeld, *Chem. Commun.* **2001**, 1376–1377.

[47] The fact that the BPh_4^- salts crystallize better than the ClO_4^- salts has been observed in other dinuclear nickel complexes supported by H_2L. It is assumed that the more polar ClO_4^- salts crystallize with more solvate molecules. Indeed, crystals of the perchlorate salts upon contact with air quickly loose the solvate molecules and turn dull.
[48] B. J. Dunne, A. G. Orpen, *Acta. Crystallogr. Sect. C* **1991**, *47*, 345–347.
[49] S.-M. Kuang, P. E. Fanwick, R. A. Walton, *Inorg. Chem.* **2002**, *41*, 1036–1038.
[50] H. Schmidbaur, S. Cronje, D. Djordjevic, O. Schuster, *Chem. Phys.* **2005**, *311*, 151–161.
[51] J. D. E. T. Wilton-Ely, A. Schier, N. W. Mitzel, H. Schmidbaur, *J. Chem. Soc. Dalton Trans.* **2001**, 1058–1062.
[52] a) N. W. Alcock, F. R. Hartley, D. E. Rogers, *J. Chem. Soc. Dalton Trans.* **1973**, 1070–1073; b) P.-K. F. Chin, F. R. Hartley, *Inorg. Chem.* **1976**, *15*, 982–984.
[53] S. H. Strauss, *Chem. Rev.* **1993**, *93*, 927–942.
[54] J. M. Forward, J. P. Fackler, Jr., R. J. Staples, *Organometallics* **1995**, *14*, 4194–4198.
[55] J. P. Fackler, R. J. Staples, A. Elduque, T. Grant, *Acta Crystallogr. Sect. C* **1994**, *50*, 520–523.
[56] X. Hong, K.-K. Cheung, C.-X. Guo, C.-M. Che, *J. Chem. Soc. Dalton Trans.* **1994**, 1867–1871.
[57] Y. Journaux, T. Glaser, G. Steinfeld, V. Lozan, B. Kersting, *Dalton Trans.* **2006**, 1738–1748.
[58] Preliminary DFT calculations have been performed for the mixed-valent $[Ni_2L(dppba)]^{2+}$ dication. These reveal an $S_{tot}={}^3/_2$ ground state that is attained by a ferromagnetic exchange interaction between a Ni^{II} ($S_1=1$) and a low-spin Ni^{III} ($S_2={}^1/_2$) ion. The $S={}^3/_2$ ground state for the $[Ni_2L(dppba)]^{2+}$ dication is also confirmed by preliminary ESR spectroscopic measurements at X-band as well as by temperature-dependent magnetic susceptibility measurements. C. Loose, J. Kortus, R. Schnorr, B. Kersting, unpublished results.
[59] A solution of the one-electron oxidized $\mathbf{2}^{2+}$ dication has been prepared by oxidation of $[Ni_2L(dppba)]ClO_4$ with one equivalent of $Cu(ClO_4)_2$. The electronic absorption spectrum of $\mathbf{2}^{2+}$ (λ_{max} (ε) = 782 (4945), 517 (2735), 397 sh (2998), 330 (9864), 304 nm ($13560\ M^{-1}cm^{-1}$) is very similar to that of $\mathbf{3}^{2+}$.
[60] *Encyclopedia of Electrochemistry of the Elements, Vol. IV* (Ed.: A. J. Bard), Marcel Dekker, New York, **1975**, p. 101.
[61] R. Uson, A. Laguna, *Organomet. React. Synth.* **1986**, *3*, 322–342.
[62] H.-J. Krueger, R. H. Holm, *Inorg. Chem.* **1989**, *28*, 1148–1155.
[63] J. D. Franolic, W. Y. Wang, M. Millar, *J. Am. Chem. Soc.* **1992**, *114*, 6587–6588.
[64] G. Henkel, T. Krüger, B. Krebs, *Angew. Chem.* **1992**, *104*, 71–72; *Angew. Chem. Int. Ed. Engl.* **1992**, *31*, 54–56.
[65] T. Beissel, T. Glaser, F. Kesting, K. Wieghardt, B. Nuber, *Inorg. Chem.* **1996**, *35*, 3936–3947.
[66] B. Kersting, D. Siebert, *Inorg. Chem.* **1998**, *37*, 3820–3828.
[67] X. E. Bill, http://www.mpibac.mpg.de/bac/logins/bill/julXen.php.
[68] We have recorded reduced magnetization data for a similar set of complexes, $[Ni_2(L)(O_2CC_6H_4SH)][ClO_4]$ and $[Ni_2(L)(O_2CC_6H_4SAuPPh_3)][BPh_4]$, but again the fits were insensitive to the value of the *D* parameter. A meaningful simulation of magnetization data for these complexes necessitates knowledge of the relative orientations of zero-field splitting tensors, which is beyond the scope of this study. J. Lach, Dissertation, Universität Leipzig, 2013.
[69] C. Golze, A. Alfonsov, R. Klingeler, B. Büchner, V. Kataev, C. Mennerich, H.-H. Klauss, M. Goiran, J.-B. Broto, H. Rakoto, S. Demeshko, G. Leibeling, F. Meyer, *Phys. Rev. B* **2006**, *73*, 224403–1–8.
[70] A. Ulman, *An Introduction to Ultrathin Organic Films from Langmuir–Blodgett to Self-Assembly*, Academic Press, New York, **1991**, pp. 237–300.
[71] The complexes cannot be deposited by using the gas phase. They decompose without melting.
[72] B. S. Sumerlin, A. B. Lowe, P. A. Stroud, P. Zhang, M. W. Urban, C. L. McCormick, *Langmuir* **2003**, *19*, 5559–5562.
[73] K. Hara, R. Akiyama, S. Takakusagi, K. Uosaki, T. Yoshino, H. Kagi, M. Sawamura, *Angew. Chem.* **2008**, *120*, 5709–5712; *Angew. Chem. Int. Ed.* **2008**, *47*, 5627–5630.
[74] K. Uvdal, I. Persson, B. Liedberg, *Langmuir* **1995**, *11*, 1252–1256.
[75] W. W. Weare, S. M. Reed, M. G. Warner, J. E. Hutchison, *J. Am. Chem. Soc.* **2000**, *122*, 12890–12891.
[76] The different solubilities of α- and β-cyclodextrin are a representative example, see: J. W. Steed, J. L. Atwood, *Supramolecular Chemistry*, 2nd ed., Wiley, Chichester, **2009**, pp. 327–336.
[77] C. D. Bain, E. B. Troughton, Y. T. Tao, J. Evall, G. M. Whitesides, R. G. Nuzzo, *J. Am. Chem. Soc.* **1989**, *111*, 321–335.
[78] M. Ratel, M. Branca, J. Breault-Turcot, S. S. Zhao, P. Chaurand, A. R. Schmitzer, J.-F. Masson, *Chem. Commun.* **2011**, *47*, 10644–10646.
[79] The sample integrity and the sensitivity to exposure to the X-ray beam while taking XPS data has been checked by a comparison of data sets that have been measured for different periods of time. For instance, after an exposure to the X-rays of a few hours only (2–3 h), no additional phosphorous signal can be observed as it is the case for longer measurements. Unfortunately, the shorter measurements do not allow a reliable analysis of the composition due to bad statistics. The small amount of material in the monolayer required long acquisition times.
[80] R. G. Copperthwaite, J. Lloyd, *J. Chem. Soc. Dalton Trans.* **1977**, 1117–1121.
[81] W. E. Swartz, Jr., J. K. Ruff, D. M. Hercules, *J. Am. Chem. Soc.* **1972**, *94*, 5227–5229.
[82] E. Fluck, D. Weber, *Z. Anorg. Allg. Chem.* **1975**, *412*, 47–58.
[83] L. Wang, D. Dehe, T. Philippi, A. Seifert, S. Ernst, Z. Zhou, M. Hartmann, R. N. Klupp-Taylor, A. P. Singh, M. Jia, W. R. Thiel, *Catal. Sci. Technol.* **2012**, *2*, 1188–1195.
[84] a) K. Velauthamurty, S. J. Higgins, R. M. G. Rajapakse, J. Bacsa, H. van Zalinge, R. J. Nichols, W. Haiss, *J. Mater. Chem.* **2009**, *19*, 1850–1858; b) E. de Wolf, A. J. M. Mens, Gijzeman, J. H. van Lenthe, L. W. Jenneskens, B.-J. Deelman, G. van Koten, *Inorg. Chem.* **2003**, *42*, 2115–2124; c) T. Borkowski, W. Zawartka, P. Pospiech, U. Mizerska, A. M. Trzeciak, M. Cypryk, W. Tylus, *J. Catal.* **2011**, *282*, 270–277.
[85] L. J. Matienzo, L. I. Yin, S. O. Grim, W. E. Swartz, Jr., *Inorg. Chem.* **1973**, *12*, 2762–2769.
[86] T. Gao, P. Norby, H. Okamoto, H. Fjellvåg, *Inorg. Chem.* **2009**, *48*, 9409–9418.
[87] I. Preda, A. Gutiérrez, A. Abbate, F. Yubero, J. Méndez, L. Alvarez, L. Soriano, *Phys. Rev. B* **2008**, *77*, 075411–1–7.
[88] An analysis of the SAM stoichiometry shows a Ni/S atomic ratio of 0.24 rather than the nominal value (0.66), which is attributed to the low intensity of the Ni and S signals.
[89] C. M. Whelan, C. J. Barnes, C. G. H. Walker, N. M. D. Brown, *Surf. Sci.* **1999**, *425*, 195–211.
[90] M. Wells, D. L. Dermody, H. C. Yang, T. Kim, R. M. Crooks, *Langmuir* **1996**, *12*, 1989–1996.
[91] *Optical Properties of Condensed Matter and Applications* (Ed.: J. Singh), Wiley, Chichester, **2006**, p. 7.
[92] S. R. Wassermann, G. M. Whitesides, I. M. Tidswell, B. M. Ocko, P. S. Pershan, J. D. Axe, *J. Am. Chem. Soc.* **1989**, *111*, 5852–5861.
[93] Others authors use $A=1.50$, which, in the case of the present monolayers, would only make a thickness difference of about 0.1 nm, see D. L. Allara, R. G. Nuzzo, *Langmuir* **1985**, *1*, 45–52.
[94] A. Ulman, *Acc. Chem. Res.* **2001**, *34*, 855–863.
[95] This value is calculated by adding the van der Waals radii of two H atoms (2.4 Å) to the atom distance of 13.123 Å.
[96] A. Reis, D. Dehe, S. Farsadpour, I. Munstein, Y. Sun, W. R. Thiel, *New J. Chem.* **2011**, *35*, 2488–2495.
[97] Under our experimental conditions $E(Cp_2Co^+/Cp_2Co) = -1.345$ V versus $E(Cp_2Fe^+/Cp_2Fe)$; $E(Cp_2Co^+/Cp_2Co) = -0.937$ V versus SCE. N. G. Connelly, W. E. Geiger, *Chem. Rev.* **1996**, *96*, 877–910.
[98] The cleaning of the substrate by the piranha solution proved necessary to obtain reasonable surface thicknesses.

[99] CompleteEase, *Software for Ellipsometry Data Aquisition and Analysis*, J. A. Wollam Co., Inc. Lincoln, NE, USA.
[100] Casa Software Ltd, Bay House 5 Grosvenor Terrace Teignmouth, TQ14 8NE, United Kingdom.
[101] Stoe, Cie, *IPDS and X-RED32* **2008**.
[102] G. M. Sheldrick, *Acta Crystallogr. Sect. A* **1990**, *46*, 467–473.
[103] G. M. Sheldrick, *SHELXL-97*, Computer program for crystal structure refinement, University of Göttingen, Göttingen, Germany, **1997**.
[104] A. L. Spek, PLATON - A Multipurpose Crystallographic Tool; Utrecht University, Utrecht, The Netherlands, **2000**.
[105] L. J. Farrugia, *J. Appl. Crystallogr.* **1997**, *30*, 565.

Received: February 7, 2013
Published online: April 17, 2013

